Available online at www.sciencedirect.com
SCIENCE DIRECT
ELSEVIER
Icarus 176 (2005) 12–43
ICARUS
www.elsevier.com/locate/icarus

Mars Exploration Rover candidate landing sites as viewed by THEMIS

P.R. Christensen [a], S.W. Ruff [a,*], R. Fergason [a], N. Gorelick [a], B.M. Jakosky [b], M.D. Lane [c], A.S. McEwen [d], H.Y. McSween [e], G.L. Mehall [a], K. Milam [e], J.E. Moersch [e], S.M. Pelkey [b], A.D. Rogers [a], M.B. Wyatt [a]

[a] *Department of Geological Sciences, Arizona State University, Box 876305, Tempe, AZ 85287-6305, USA*
[b] *Laboratory for Atmospheric Physics, University of Colorado, Boulder, CO 80309, USA*
[c] *Planetary Science Institute, Tucson, AZ 85719-2395, USA*
[d] *Lunar and Planetary Laboratory, University of Arizona, Tucson, AZ 85721, USA*
[e] *Department of Geological Sciences, University of Tennessee, Knoxville, TN 37996-1410, USA*

Received 23 December 2003; revised 23 December 2004

Available online 17 March 2005

Abstract

The analysis of six landing sites that were candidates for the two NASA Mars Exploration Rovers (MER) benefited from recently available image data from the Thermal Emission Imaging Spectrometer (THEMIS) onboard the 2001 Mars Odyssey spacecraft. The combination of daytime and nighttime thermal infrared images from THEMIS supplemented by additional data sets has lead to new or expanded insights into the nature of each landing site. In Meridiani Planum, a layer of lighter-toned, higher thermal inertia material is observable just below the hematite-bearing layer. Gusev Crater displays a more complex stratigraphy than previously observed, including an upper layer with lobate margins. The highest inertia unit of southern Isidis Planitia is confined to topographic lows in the rim/basin margin and does not appear to be due to highland material transported onto the basin floor. The enigmatic, ovoid, blocky terrain on the floor of Melas Chasma displays higher thermal inertia than its surroundings, an indication that it contains coarser or more indurated material than the adjacent aeolian bedforms. The myriad channels of Athabasca Valles display distinctive thermal signatures despite the presence of a bright layer of dust covering the region. The presence of alluvial fans produced from spur-and-gulley erosion of the walls of Eos Chasma demonstrates that mass movements have occurred following the canyon scouring floods.

Keywords: Mars, surface; Infrared observations

1. Introduction

In June and July of 2003 NASA launched two spacecraft bound for two different landing sites on the martian surface. Each carried an identical payload called the Mars Exploration Rover (MER) (Crisp et al., 2003), a mobile platform with a suite of instruments designed to characterize the geology, mineralogy, and surface chemistry within ∼1 km of the point of touchdown (Squyres et al., 2003). One hundred eighty-five potential landing sites satisfied the initial engineering constraints (Golombek et al., 2003). Many fewer satisfied the broad scientific aim of landing at a location with evidence of an aqueous history. Reducing the list was a winnowing process intended to accommodate both scientific interests and engineering constraints (Golombek et al., 2003). Based upon information derived mostly from Mars Global Surveyor and Viking data sets, the list of sites had been reduced to 6 candidates by October of 2001. By January 2002, the 4 primary sites were Meridiani Planum, Gusev Crater, Isidis Planitia, and Melas Chasma, with 2 backup sites at Athabasca Valles and Eos Chasma. Each encompassed an elliptical region with dimensions ranging from 95–155 km on the long axis and 16–20 km on the short axis (Golombek et al., 2003).

* Corresponding author.
E-mail address: steve.ruff@asu.edu (S.W. Ruff).

0019-1035/$ – see front matter
doi:10.1016/j.icarus.2005.01.004

The 2001 Mars Odyssey spacecraft arrived in orbit around Mars in February of 2002 and began observing the planet with a set of three instruments. One of these instruments, the Thermal Emission Imaging System (THEMIS), is well suited to providing additional information about the MER landing sites. THEMIS is a multi-spectral imager with 9 different bands in the thermal infrared (IR) wavelengths (6.78, 7.93, 8.56, 9.35, 10.21, 11.04, 11.79, 12.57, and 14.88 μm) and 5 bands in the visible/near infrared wavelengths (0.425, 0.540, 0.654, 0.749, and 0.860 μm) (Christensen et al., 2004). The two different wavelength regions are measured by two separate camera systems resulting in a different spatial resolution and coverage for each. The IR camera produces images with a resolution of ∼100 m/pixel spanning ∼32 km in the cross track dimension and a variable down track dimension. The VIS (visible imaging subsystem) camera is bore-sighted with the IR camera, producing images nested within the IR image frame having ∼19 m/pixel spatial resolution, a cross track dimension of ∼19 km and a variable down track dimension.

With the commencement of THEMIS mapping operations, the 6 candidate landing sites were targeted at every opportunity. Both daytime (∼1500–1700 local time) and nighttime (∼0300–0500 local time) IR images as well as daytime VIS images in multiple band passes were acquired. Each landing ellipse has nearly complete contiguous coverage in both wavelength regions. By June of 2002, three of the 6 sites had been removed from further consideration due to landing safety concerns (Athabasca, Melas, and Eos) and by time of launch, Gusev and Meridiani were the designated finalists. However, because all 6 sites have received a significant investment of scientific inquiry and resources, an analysis of each is included in this paper. The scientific interest in the four eliminated sites remains undiminished despite the landing safety drawbacks. More robust landing systems may allow these sites to be visited by future spacecraft.

For each of the 6 sites, a brief rationale is given for its inclusion among the final candidates along with a description of the site's geological setting. In all cases, "landing site" connotes the broader context in which the actual landing ellipse occurs. Daytime and nighttime mosaics of THEMIS IR images converted to brightness temperature are the focus of the analysis for each site, supplemented by observations from THEMIS VIS, Viking, and Mars Global Surveyor Mars Orbiter Camera (MGS-MOC) images. Observations that are unique to or more clearly presented by the THEMIS data set are emphasized. The mosaics have been produced from geometrically rectified and radiometrically calibrated THEMIS images. Both daytime and nighttime IR mosaics use band 9 (12.57 μm) data because of its high signal to noise ratio (SNR) and the relative transparency of the martian atmosphere in this wavelength region. The data are displayed in grayscale, resulting in images that show a range of intensities where bright tones indicate warmer temperatures than dark tones. Because each image strip in the mosaics has been normalized, the grayscale intensities represent relative temperature variations.

Single band, daytime IR images are well suited for the analysis of geomorphology because variations in topography and albedo give rise to the most significant radiance/temperature variations seen in the images (Christensen et al., 2003). THEMIS VIS images provide additional details, supplementing the coverage by the Mars Global Surveyor and Viking cameras. In the nighttime IR images, topography and albedo effects are diminished significantly, revealing variations largely attributable to thermal inertia (Christensen et al., 2003). These images therefore are useful for discerning variations in particle size or degree of induration of surface materials. While multispectral images have been acquired for the landing sites (both IR and VIS), this paper focuses on single-band images because the band-to-band registration and calibration necessary for compositional analysis was not implemented fully at the time of writing.

2. Landing site analyses

2.1. *Meridiani Planum*

Meridiani Planum (formerly known as Sinus Meridiani and Terra Meridiani) emerged as a candidate landing site following the discovery of gray crystalline hematite from IR spectra measured by the MGS Thermal Emission Spectrometer (TES) (Christensen et al., 2000). Water likely was involved in the formation of the hematite deposit although the role it played remains the subject of debate (e.g., Christensen et al., 2000, 2001; Hynek et al., 2002; Newsom et al., 2003). The apparent association with water makes Meridiani Planum an appealing target for in situ investigation. The hematite is found in an irregularly shaped deposit centered at ∼357° E and 2° S spanning roughly 500 km in the E–W direction and 300 km N–S. It is associated with a relatively smooth plains material that appears to mantle the underlying terrain. Based on observations from Viking and MOC images, it is apparent that the hematite is hosted within friable, layered sediments (e.g., Presley and Arvidson, 1988; Edgett, 1997; Christensen et al., 2000; Hynek et al., 2002). These sediments comprise a regionally extensive stratigraphic sequence that has undergone major erosion (e.g., Hynek et al., 2002). The nature of the sedimentary materials is enigmatic. Although it has been recognized that the hematite unit is dominated by material with a basaltic composition (Christensen et al., 2001), it is not clear what sedimentary processes have produced the layered sequence. While some form of volcanic air fall or pyroclastic deposits are potential candidates (e.g., Chapman and Tanaka, 2002; Hynek et al., 2002), a subaqueous origin cannot be ruled out.

The Meridiani hematite deposit is well suited to a landing site. Its smooth, flat surface and average rock abundance

of ∼7% (Christensen et al., 2000) provide a safe surface upon which to land and conduct rover operations. Within the landing ellipse, albedo values with a range of ∼0.14–0.19 and dust cover index (DCI) values from ∼0.96–0.98 demonstrate that this is a location with little dust accumulation (Ruff and Christensen, 2002). The TES-derived values of thermal inertia (Mellon et al., 2000) range from ∼150–400 J m^{-2} s$^{-1/2}$ K^{-1} (physical units are omitted hereafter).

2.1.1. THEMIS daytime IR

A THEMIS mosaic containing the landing site ellipse (Fig. 1) shows variations in daytime temperature that likely are due to differences in thermal inertia values across the

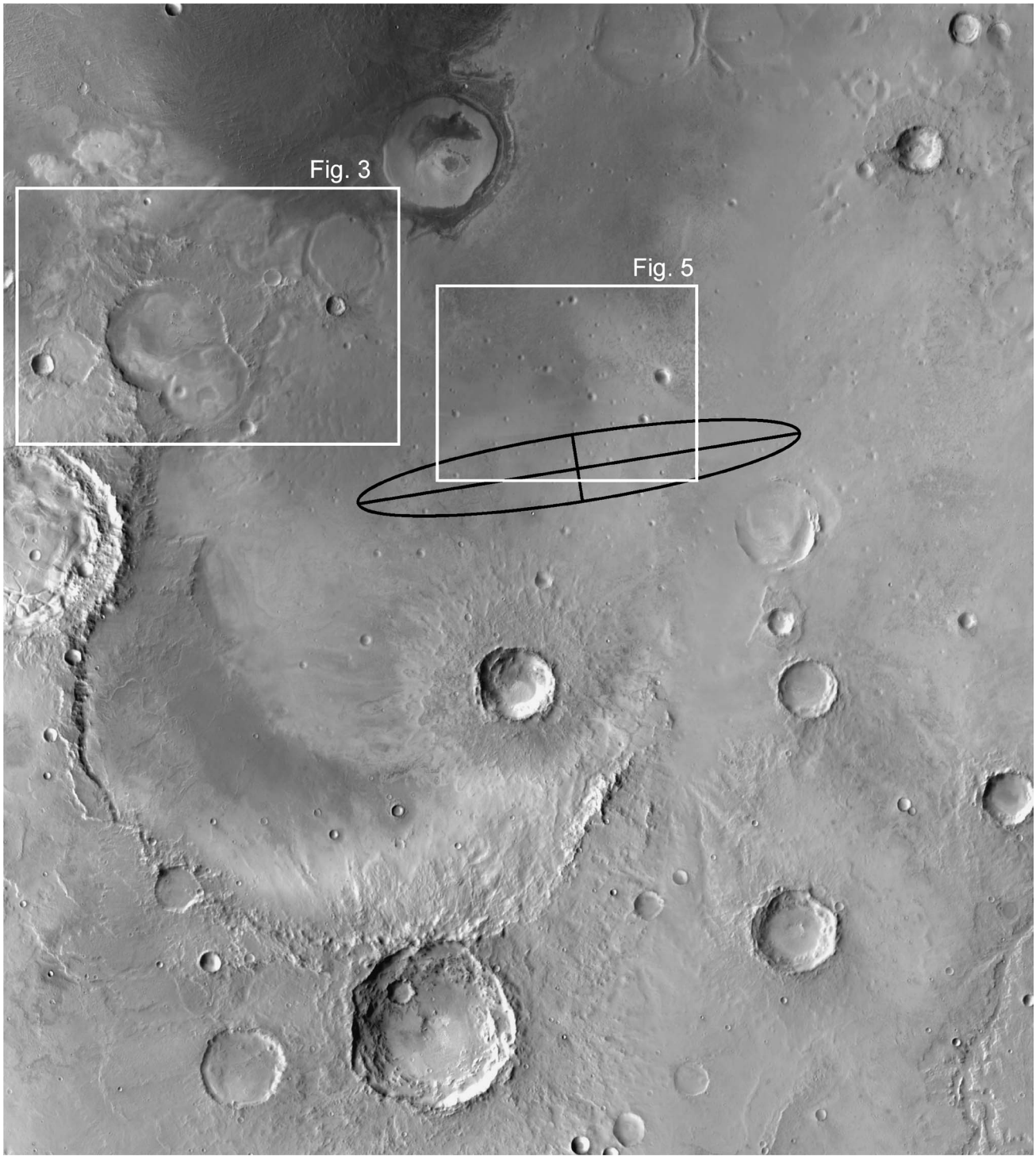

Fig. 1. A mosaic of THEMIS band 9 daytime IR temperature data covering the region of the Meridiani Planum landing site. The mosaic is centered at 2.0° S, 354.1° E. The intended landing ellipse is shown in black and has a semi-major and semi-minor axis of 117 and 18 km, respectively.

scene (Christensen et al., 2003). A comparison of the distribution of TES-based hematite abundance (Fig. 2) and the THEMIS mosaic reveals a remarkable correlation between the hematite-bearing unit and surfaces that appear relatively smooth and warm in the daytime mosaic. This is especially apparent along the northwest margin of the hematite deposit where the hematite-bearing unit occurs in isolated patches associated with filled craters and intercrater mesas (Fig. 3). These occurrences provide further details about the stratigraphy and characteristics of the sedimentary layers that include the hematite deposit. An example is the partially exhumed crater pair due west of the landing ellipse (Fig. 3). TES data in this location show that hematite occurs within the warmer layer but is absent from all of the patches that appear cooler in the daytime IR image. A THEMIS VIS image that covers a portion of this scene (Fig. 4) shows that the hematite layer evident from TES data overlies an etched surface of partially streamlined buttes, an observation consistent with similar observations by Hynek et al. (2002). It appears that the hematite-rich sediment was deposited directly on top of a surface that already had been heavily eroded, suggesting a significant hiatus between the deposition of hematite-poor and hematite-rich sediments.

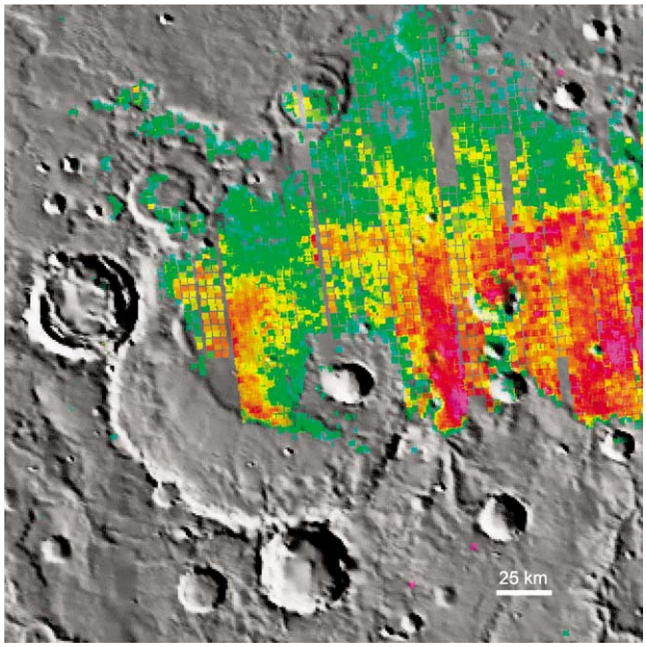

Fig. 2. TES hematite index in Meridiani Planum overlain on MOLA shaded relief topographic data centered at 2.7° S, 353.5° E. The colored TES data represent the hematite index from Christensen et al. (2000) mapped at full spatial resolution. The index shows relative hematite abundance in colors ranging from greenish hues (least abundant) to reddish hues (most abundant).

Within the landing ellipse, variations in daytime temperatures are minor ($< \sim 5$ K) although still apparent. A relatively cool patch toward the center of the ellipse has a streaked appearance in the E–W direction suggestive of wind activity (Fig. 5). Along the northeast portion of the ellipse, the surface appears significantly mottled (Fig. 5). The relatively warm, smooth surface that dominates the ellipse appears fragmented in this location with cooler surfaces in the

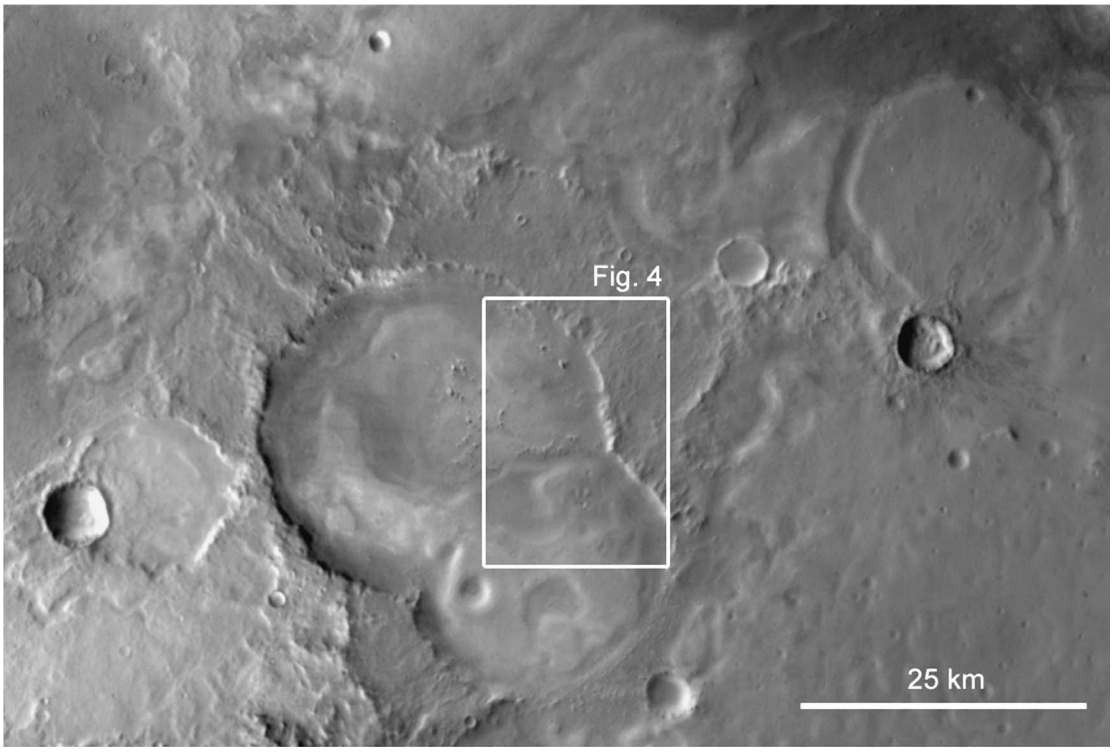

Fig. 3. The northwest margin of the hematite-bearing unit centered at 1.4° S, 352.4° E in Meridiani Planum enlarged from the THEMIS daytime IR mosaic of Fig. 1. Hematite is associated with the brighter, topographically higher surfaces in the scene.

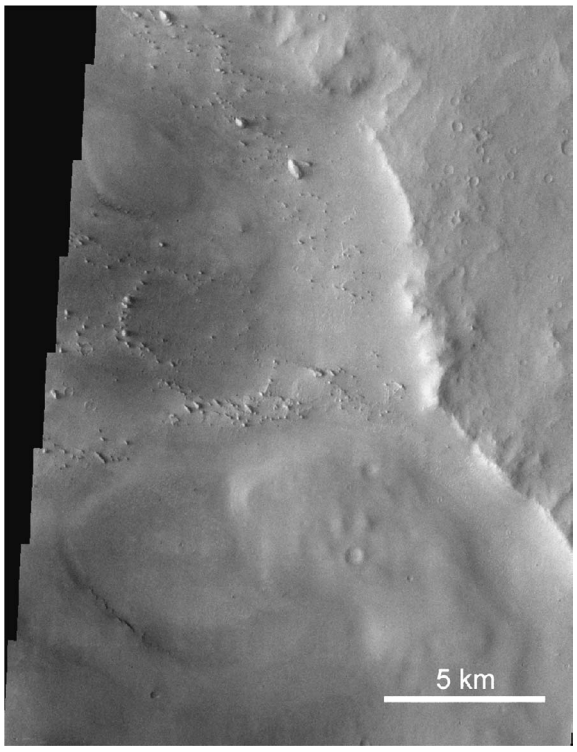

Fig. 4. A subframe of THEMIS VIS image V05993001 centered at 1.5° S, 352.4° E showing a portion of the Meridiani Planum scene from Fig. 3. Hematite occurs in the hummocky terrain in the southern portion of the image based on the distribution of hematite seen in Fig. 2. The hematite-bearing material appears to overlie a former surface of eroded buttes.

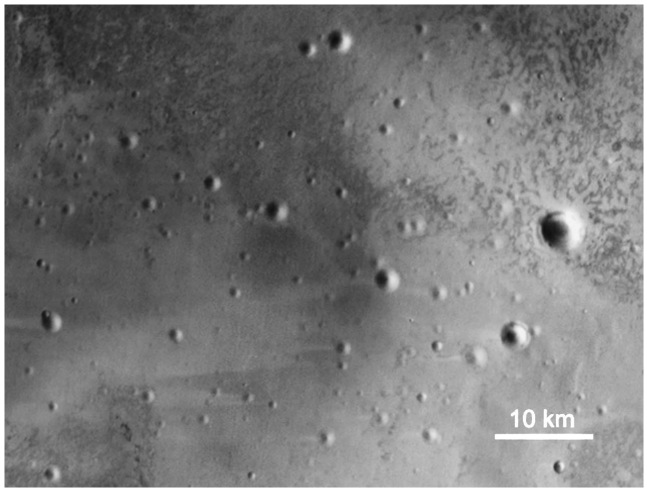

Fig. 5. An enlarged portion of the THEMIS daytime IR mosaic of Fig. 1 centered at 1.7° S, 353.9° E showing the streaked and mottled surface within the boundary of the Meridiani Planum landing ellipse.

interstices. More discussion of this area is given in the next section. There are a few dozen small craters (< ∼5 km diameter) within the ellipse that appear in the daytime IR image by virtue of differential slope heating (Fig. 5). All of these craters lack a raised rim and show no sign of ejecta, likely indicating post-emplacement modification.

2.1.2. THEMIS nighttime IR

Most of the features evident in the daytime IR mosaic are present in the nighttime mosaic (Fig. 6) but with a reversal in temperature contrast. Such behavior strongly suggests that thermal inertia rather than albedo or topographic effects dominates both the daytime and nighttime IR temperature variations (Christensen et al., 2003). Relative thermal inertia of the different surface units can be evaluated directly from the nighttime mosaic. The surfaces that contain hematite (see Fig. 2) are among the coolest in the entire scene, an indication that they have relatively low thermal inertia. This is especially apparent in the westernmost portion of the hematite deposit and among the isolated patches of hematite in the filled craters and intercrater mesas along the northwest boundary. Conversely, the surfaces that underlie the hematite layer are among the warmest nighttime IR features. The partially exhumed crater pair due west of the landing ellipse described in the previous section (Fig. 3) clearly demonstrates the nighttime IR characteristics of the hematite layer and underlying etched layer: the former is cooler compared with the latter. Therefore the lower, etched layer has higher thermal inertia than the hematite layer, an observation noted by Arvidson et al. (2002, 2003).

Elsewhere in the scene there is additional evidence that a higher thermal inertia layer is present under the hematite-rich layer. The low scarp that marks the westernmost boundary of the hematite deposit is one example. This location shows a thin band of relatively warm material that is conformal with the scarp (Fig. 7) and appears cooler in the daytime IR mosaic. These observations tend to support the idea that the hematite layer buries material with a higher thermal inertia. This idea is further supported by other observations. Just to the north of the approximate center of the ellipse are two rimless craters roughly 4 and 5 km in diameter (Fig 8) with characteristics similar to those described by Koeppen et al. (2003). Each shows a collar of relatively warm material that extends approximately 3/4 of the way around the lip of the crater. A THEMIS VIS image reveals the morphologic and albedo characteristics of these craters (Fig. 9). At the lip of each crater, the smooth surface of the hematite layer is disrupted, apparently revealing visibly brighter material below. This contrasts with the southern portion of these two craters where the hematite layer makes a smooth transition into the bowl of each crater. In this portion there is neither a change in apparent albedo or temperature. An interpretation of these observations is that the hematite layer is so thin that it is susceptible to erosion that can strip it away to reveal the underlying higher inertia unit. This susceptibility to erosion may explain the mottled surface in Figs. 5, 8, and 9.

2.1.3. Discussion

THEMIS image data of the Meridiani Planum region present a view that is consistent with previous data sets yet provides some additional insights. The hematite layer has sharp boundaries that conform to geomorphic fea-

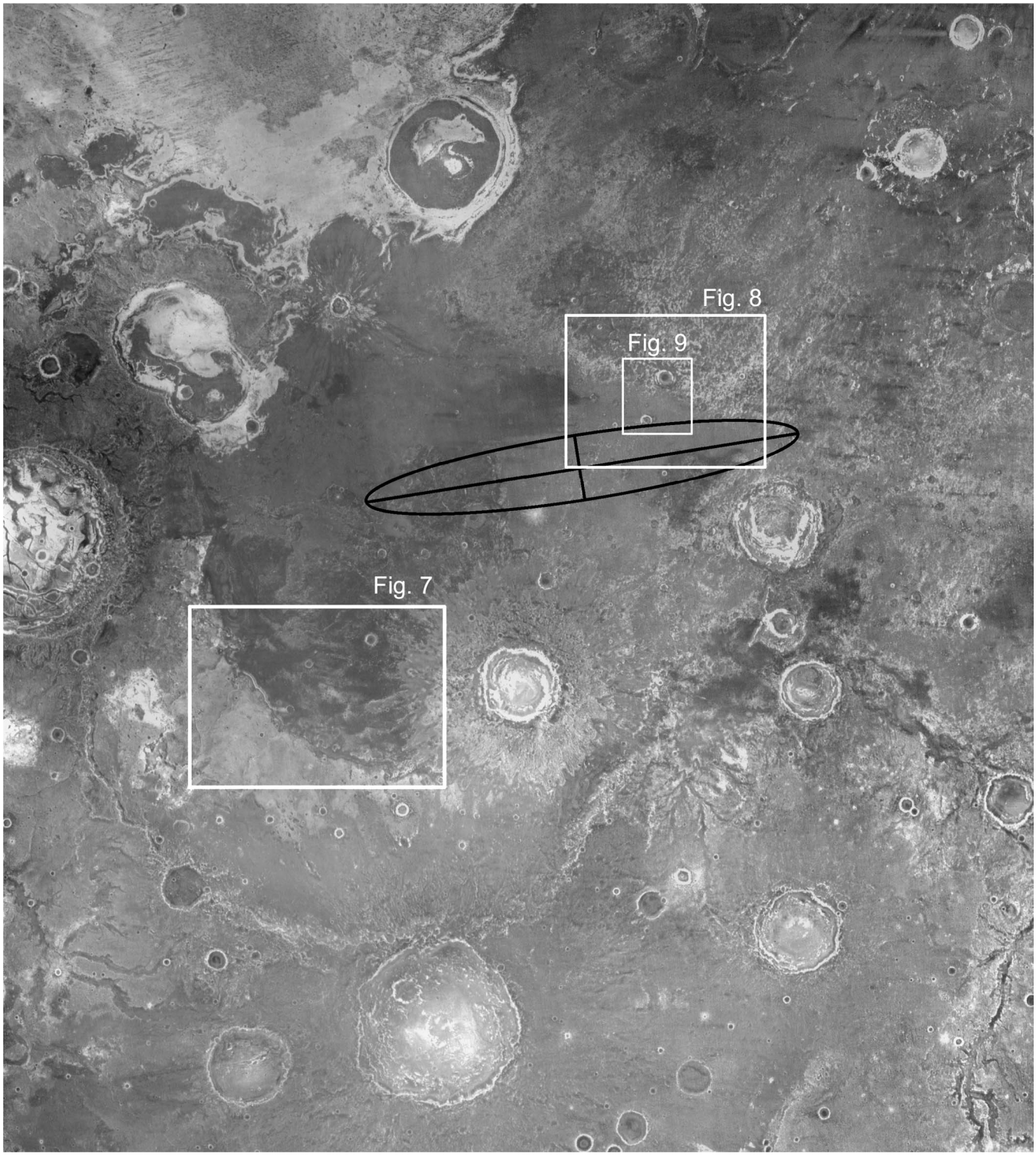

Fig. 6. A mosaic of THEMIS band 9 nighttime IR temperature data covering the region of the Meridiani Planum landing site. The mosaic is centered on 1.7° S, 353.9° E. The intended landing ellipse is shown in black and has a semi-major and semi-minor axis of 117 and 18 km, respectively.

tures. The material that contains the hematite buries a pre-existing erosional surface that likely was composed of layered sediments. Material with higher thermal inertia than the hematite-bearing layer lies just beneath the hematite surface. In places, this material clearly is associated with etched or eroded sediments below the hematite layer. In other places it appears as rims around buried craters and as mottling across otherwise smooth surfaces. Given the ubiquity of the higher inertia material throughout the region and the apparent thinness of the hematite layer, it seems likely that at least two

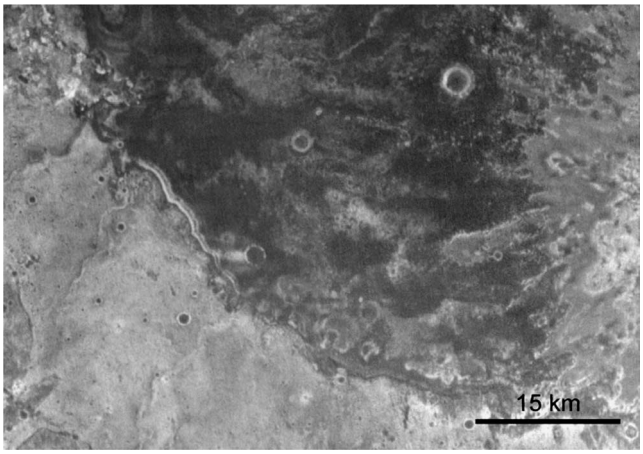

Fig. 7. An enlarged portion of the THEMIS nighttime IR mosaic of Meridiani Planum (Fig. 6) centered at 3.0° S, 352.8° E showing an exposed layer of warmer (brighter) material along the edge of the hematite-bearing unit.

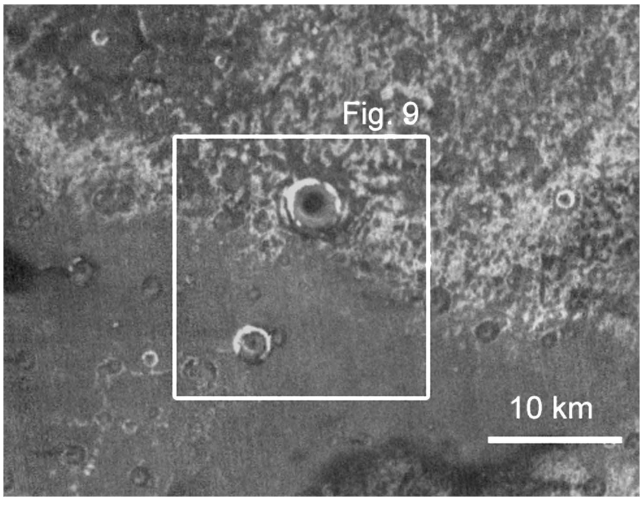

Fig. 8. An enlarged portion of the THEMIS nighttime IR mosaic of Meridiani Planum (Fig. 6) centered at 1.7° S, 354.3° E showing two rimless craters with a collar of warmer (brighter) material.

different stratigraphic units will be accessible to the rover (Koeppen et al., 2003).

2.2. Gusev Crater

Previous studies have suggested that the 160-km diameter Gusev impact crater was once filled with water (e.g., Grin and Cabrol, 1997; Cabrol et al., 1998), making it a prime candidate landing site for the Mars Exploration Rovers. The primary source of water and sediments would have been Ma'adim Vallis, a large channel spilling onto the floor of Gusev Crater. The channel and crater cut cratered plains materials of Noachian age (Kuzmin et al., 2000). The interior units of Gusev have been interpreted as deposits from multiple fluvial resurfacing events during the Noachian, Hesperian, and early Amazonian periods (Grin and Cabrol, 1997). Water appears to have exited Gusev through several gaps in the northwest rim (Kuzmin et al., 2000).

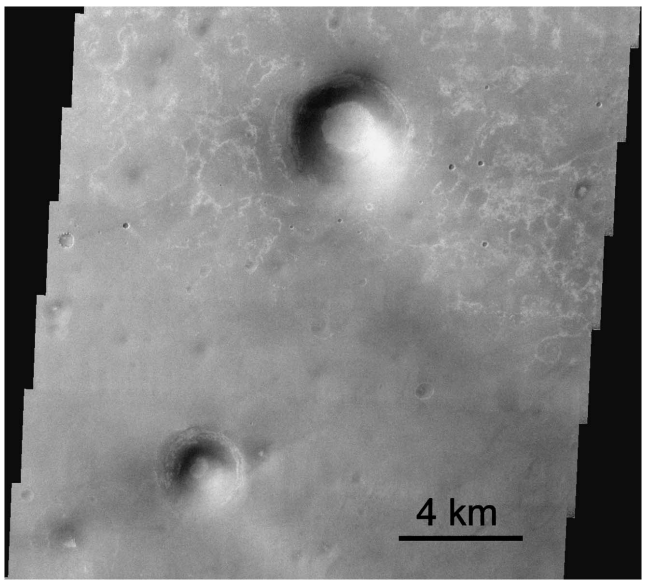

Fig. 9. A subframe of THEMIS VIS image V01836001 centered at 1.7° S, 354.3° E showing a portion of the Meridiani Planum scene from Fig. 8. The two prominent craters have rim features that coincide with those in the nighttime IR image of Fig. 8.

Geomorphic and topographic features in Gusev and Ma'adim Vallis are critical to the hypothesis that water emptied and ponded periodically in the basin. MOLA topography of Gusev indicates the basin lies as much as 2500 m below the adjacent highlands. Details in Viking images suggest terraces are present within Gusev, while a distinct set of mesas at the mouth of Ma'adim Vallis has been proposed to be a dissected delta, and morphologic features of Gusev's floor deposits have been attributed to currents in an ice-covered lake (Grin and Cabrol, 1997). Higher-resolution MOC images of Gusev, however, reveal no obvious shorelines or other lacustrine geomorphic features.

Pre-THEMIS mapping shows that most of the landing ellipse contains Members 1 and 2 of the Gusev Crater formation (Kuzmin et al., 2000), interpreted as fluvio-lacustrine deposits and debris flows. At the east end of the ellipse is the moderately degraded Thira Crater. Smooth, probably aeolian material covers much of the western end of the ellipse (Kuzmin et al., 2000). TES albedo values for the floor of Gusev range from ~0.17 to 0.26 while DCI values range from ~0.93 to 0.97. Such values are indicative of surfaces that range from dust-covered to dust-free (Ruff and Christensen, 2002). The thermal inertia values, which range from ~150 to 500, indicate that although dust may be present, it is not thick enough to fully obscure the thermal signature of the underlying substrate. The lowest-albedo, least-dusty material exhibits TES spectral properties similar to Surface Type 1 (basalt) (Milam et al., 2003); TES observations of other units in the landing ellipse are obscured by dust.

THEMIS daytime IR, nighttime IR, and VIS images reveal the terrain within Gusev Crater to possess a complex mix of features that probably have resulted from multiple depositional/erosional processes. A detailed description of

mapable units and inferred stratigraphy, based primarily on THEMIS images taken in and around the landing ellipse, can be found in Milam et al. (2003). Here we present an overview of the types of features found in THEMIS images of Gusev and a brief discussion of the processes that could have formed them.

2.2.1. THEMIS IR and VIS

The daytime IR mosaic is dramatically different from the nighttime version in its depiction of topography (Figs. 10 and 11). Differential heating of slopes produces a clear picture of the crater rim, Ma'adim Vallis, and the mesas in the south. The floor of Gusev however, displays temperature variations that are independent of topography. For example, there are two prominent streaks trending SSE that are warmer in the day by several degrees than the rest of the crater floor. These correspond to relatively low albedo streaks that are evident in visible images. Their warmer temperatures are due to the differential heating that results from albedo contrast. In MOC images as well as THEMIS VIS images (e.g., Fig. 12), these features are seen to be composed of hundreds of small, superimposed, subparallel streaks that clearly are aeolian in origin. It is unclear however, whether these features represent deposits of dark windblown sediment or areas where a thin layer of bright, fine-grained dust has been stripped off to reveal a darker substrate. The fact that the streaks are nearly indiscernible in the nighttime IR mosaic (Fig. 11) tends to support the latter idea. What is clear is that the features are dynamic; comparison with visible-wavelength images from Viking and MGS (Fig. 13) shows that the geographic boundaries of the features have changed significantly over the >20 years separating the two missions (e.g., Greeley et al., 2003b).

Between the two streaks are several 1- to 5-km sized patches that appear cooler than their surroundings in the daytime and warmer in the nighttime images (Label B in Figs. 10 and 11). THEMIS VIS images (Fig. 12) show that these features have no albedo contrast with their surroundings. The presence of daytime cool features that lack any corresponding albedo contrast indicates that they have a higher thermal inertia than the surrounding material, a suggestion supported by the warmer nighttime temperatures. The apparent constant albedo across these features combined with an apparent thermal inertia heterogeneity suggests that the area may be mantled uniformly in aeolian material, but with a thickness less than the diurnal thermal skin depth. VIS images do show a distinctive morphology that is coincident with the higher thermal inertia features. It is characterized by an etched appearance with small knobs and mesas superimposed upon a flat underlying surface. In some places, these features appear to be topographically lower than the surrounding plains, suggesting that overlying plains material may have been stripped away to reveal higher thermal inertia material beneath. Similar etched morphology is found in much larger expanses south and east of the ellipse and is coincident with relatively cool daytime and warm nighttime temperatures (Figs. 10 and 11).

The rim of 22-km Thira Crater occupies the extreme eastern end of the landing ellipse. While the Sun-facing portions of the rim are warmer due to solar heating, the SSW segment displays surfaces that are relatively warm without being sun-facing. Based on their patchy appearance and comparison with THEMIS VIS images, it appears that these are areas where either (1) dark aeolian material has been trapped on the flanks of topographic highs, or (2) bright fine-grained material has been stripped away from the surface where topographic highs are exposed to higher winds. The stratigraphic column of Milam et al. (2003) indicates that Thira rim contains the oldest material in the landing ellipse, which could include sediments from the very early floor of the Gusev basin.

The plains surrounding the aforementioned features are relatively densely populated with small (<1 km) impact craters. Milam et al. (2003) divided these plains into four mapped units, each of which extends well beyond the limits of the ellipse. However, for the purpose of understanding the features of surfaces within the ellipse, these plains can be divided into two regions. Plains in the western two-thirds of the ellipse appear distinctly warmer in the daytime IR mosaic (Fig. 10) than plains in the eastern one-third of the ellipse. This temperature contrast of a few degrees is less distinct at night (Fig. 11). However the nighttime IR mosaic does show some regional differences in the appearance of small craters. There is a tendency for small craters in the western half of Gusev to have warmer rims compared with those in the eastern half. This may indicate a difference in the age or degradation of these two crater populations, or it may indicate that they sample two different types of subsurface materials.

2.2.2. Discussion

The THEMIS observations presented above point to an interesting history of depositional and erosional processes operating within the Gusev Crater landing ellipse. The timing of these processes encompasses much of Mars' history, from initial formation of the crater in the Noachian, up through present time. While an aqueous history in Gusev has been reasonably well established, THEMIS data do not provide definitive evidence for a paleolake. Aeolian processes dominate present-day modifications of the surface, as evidenced by changing albedo patterns over the last 25 years. The processes that have lead to the observed substantial basin infilling and erosion are less certain. Aqueous and/or aeolian processes certainly are candidates, but volcanoclastic deposition also must be considered given the close proximity of Apollinaris Patera $\sim$350 km to the north.

2.3. Isidis Planitia

The candidate landing site at the southern edge of the Isidis Planitia basin was the last to be eliminated from

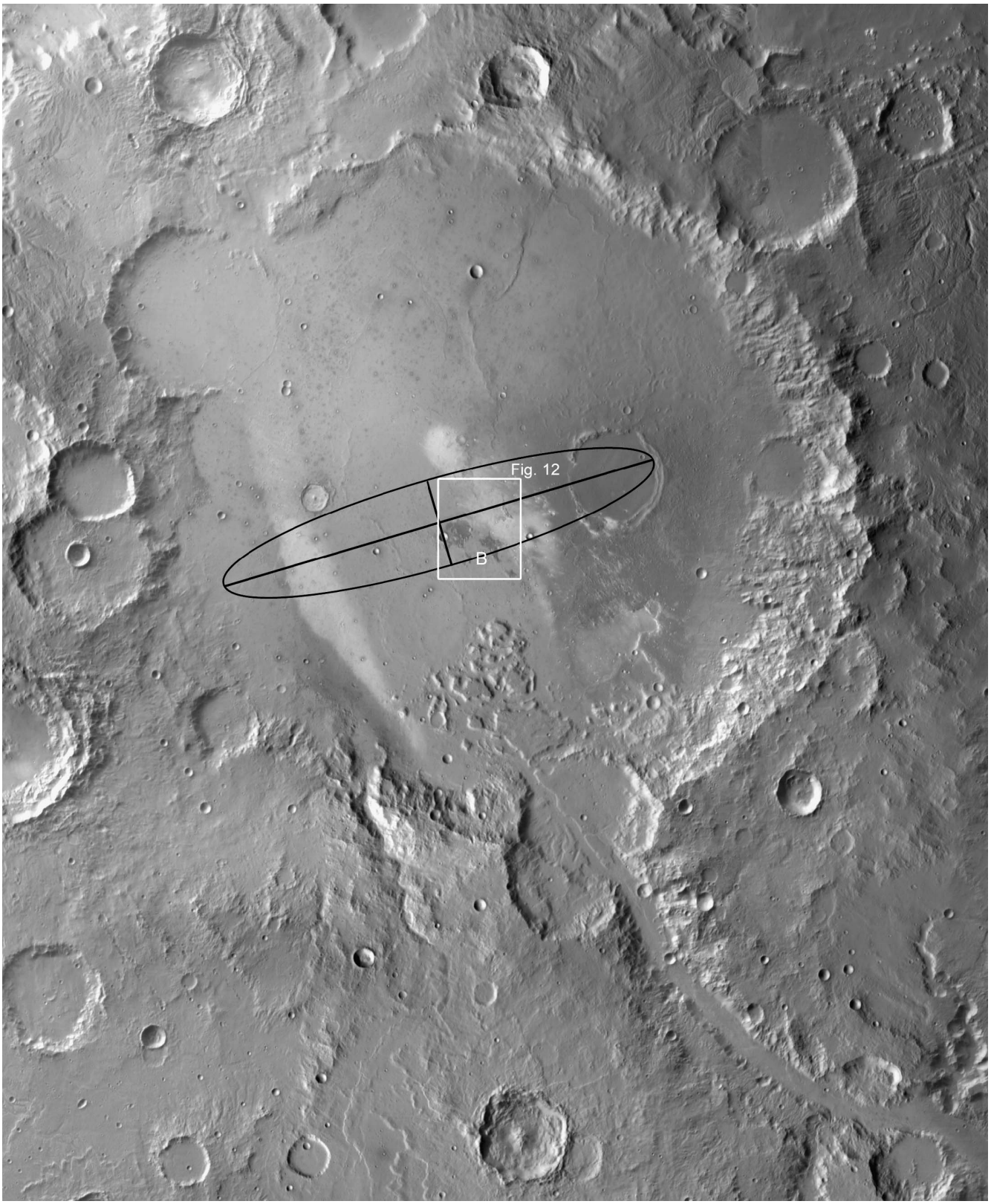

Fig. 10. A mosaic of THEMIS band 9 daytime IR temperature data covering the region of the Gusev Crater landing site. The mosaic is centered at 15.0° S, 175.5° E. The intended landing ellipse is shown in black and has a semi-major and semi-minor axis of 96 and 19 km, respectively.

consideration. Because less has been published about this location than the Meridiani and Gusev locations and because THEMIS images provide useful new views, a thorough analysis is presented here. Isidis Planitia forms the

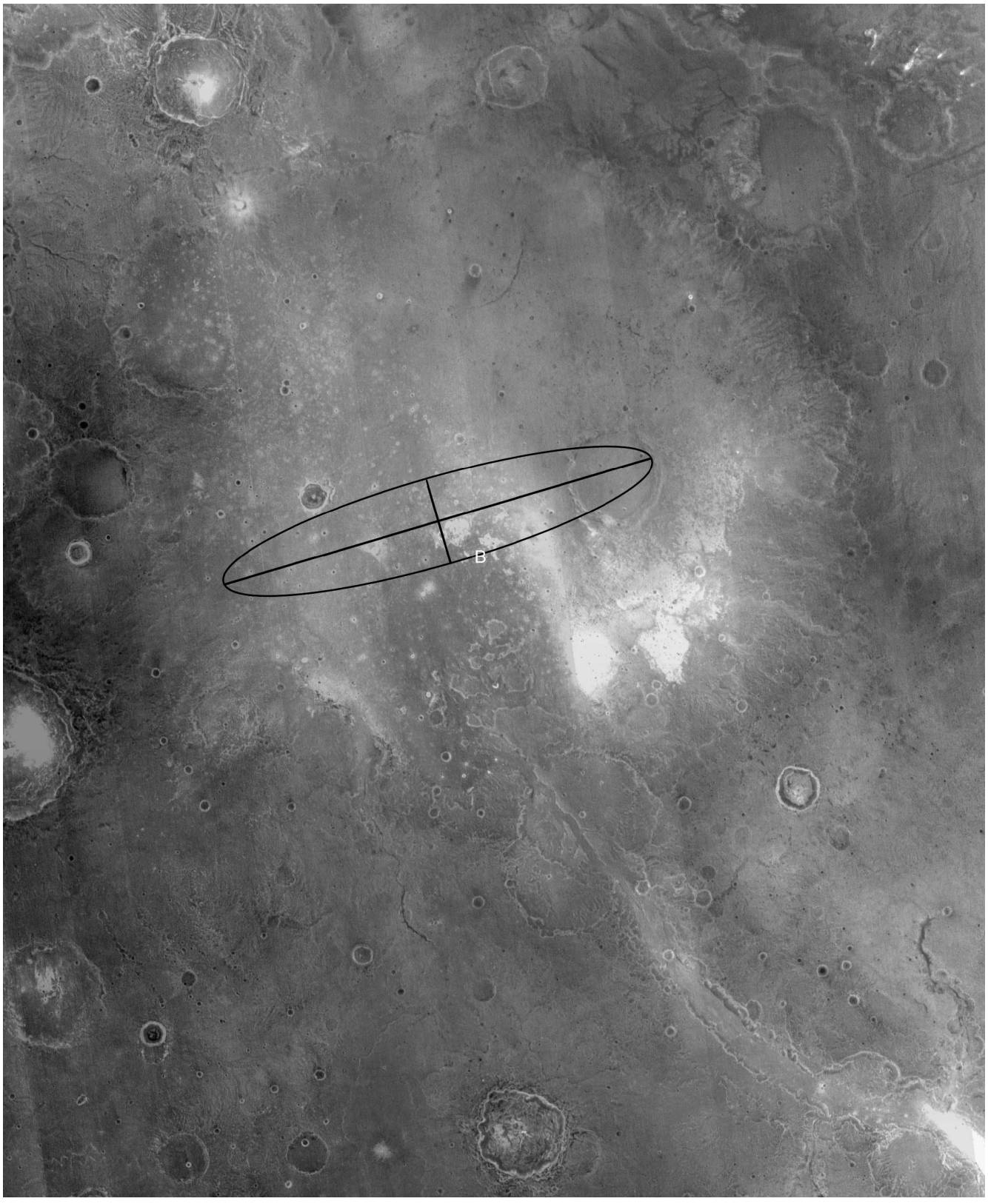

Fig. 11. A mosaic of THEMIS band 9 nighttime IR temperature data covering the region of the Gusev Crater landing site. The mosaic is centered at 15.0° S, 175.5° E. The intended landing ellipse is shown in black and has a semi-major and semi-minor axis of 96 and 19 km, respectively.

floor of an ancient impact basin. From the Libya Montes area along the southern rim down into the basin center, there is roughly 5 km's of elevation difference. De-trended MOLA topography of the basin floor shows wrinkle-ridge

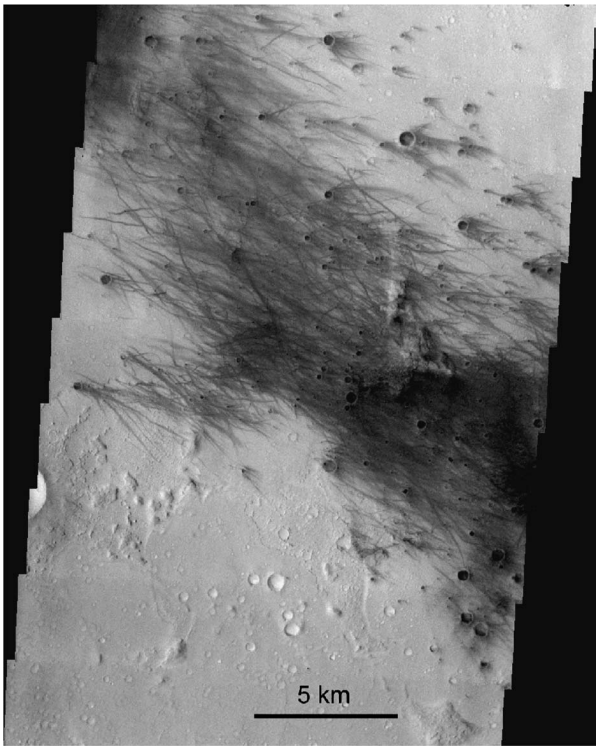

Fig. 12. A subframe of THEMIS VIS image V00881003 centered at 14.6° S, 175.5° E showing wind streaks in Gusev Crater. To the south of the wind streaks are morphologic features that show distinctive IR characteristics.

morphology that mimics the ridges found in some lunar maria (Head et al., 2002). The southern edge of Isidis Planitia was selected as a candidate landing site because of its proximity to adjacent ancient highland terrain that has been heavily dissected, probably by flowing water (Golombek et al., 2003). One hypothesis states that the observed channels have transported ancient highland material into the basin (Crumpler and Tanaka, 2003). The relatively high thermal inertia (e.g., Mellon et al., 2000) and IRTM rock abundance (Christensen, 1986) observed in this portion of the basin have been cited as evidence for the deposition of material transported via the observed drainages (Crumpler and Tanaka, 2003). Access to potential aqueously altered, ancient highland material transported into the vicinity of the ellipse is a rationale for landing at this location.

Typical TES-derived thermal inertia values within the ellipse range from 310 to 400. Adjacent to the ellipse, thermal inertia values of 500 to 690 are observed in confined areas. IRTM rock abundance near the southern Isidis rim is ∼20% (Christensen, 1986) (similar to the locations of previous landers); higher resolution TES-derived rock abundance for this area is ∼10–14% (Nowicki and Christensen, 2002). It is therefore likely that rocks at the surface are not significantly contributing to the high thermal inertia in this region and instead, the fine component is coarse-grained. Within the landing ellipse, TES-derived albedo spans the narrow range of ∼0.21 to 0.24 suggesting that a thin layer of dust covers the area. DCI values are variable throughout the ellipse (∼0.94–0.97), possibly indicating a thin or patchy covering of dust (Ruff and Christensen, 2002).

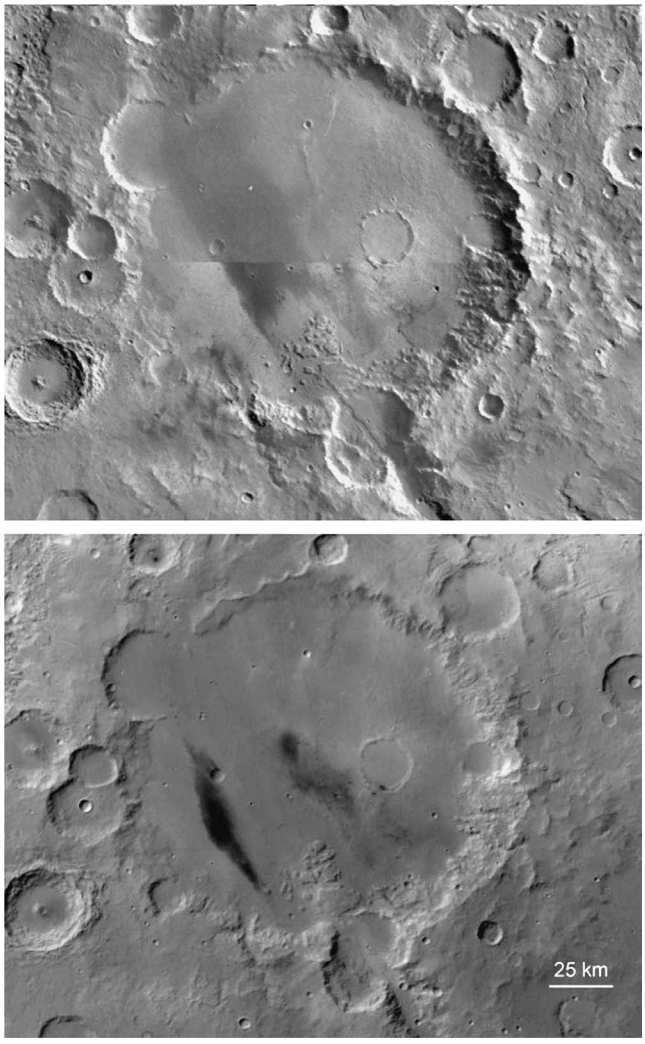

Fig. 13. Mosaics of Viking (top) and MOC wide-angle (bottom) images of Gusev Crater centered at 14.6° S, 175.5° E showing the change with time of the albedo features on the floor of the crater.

2.3.1. THEMIS IR

The rugged topography of the Libya Montes gives rise to very different views between the daytime and nighttime mosaics of the region (Figs. 14 and 15). Differential heating of slopes produces a dramatic view of topography in the daytime mosaic that is almost indiscernible at night. Careful examination of both IR mosaics along with VIS images yields several distinctive units that can be mapped on the basis of their thermophysical characteristics. These are described in the next section.

The THEMIS daytime IR mosaic provides greater detail of the morphology of the basin rim than has been available previously. The rim terrain is densely dissected by channels. Small drainage networks (an average valley width of 0.5 km), previously noted by Carr (1996) from analysis of

Fig. 14. A mosaic of THEMIS band 9 daytime IR temperature data covering the region of the Isidis Planitia basin landing site. The mosaic is centered at 3.93° N, 88.0° E. The intended landing ellipse is shown in black and has a semi-major and semi-minor axis of 135 and 16 km, respectively.

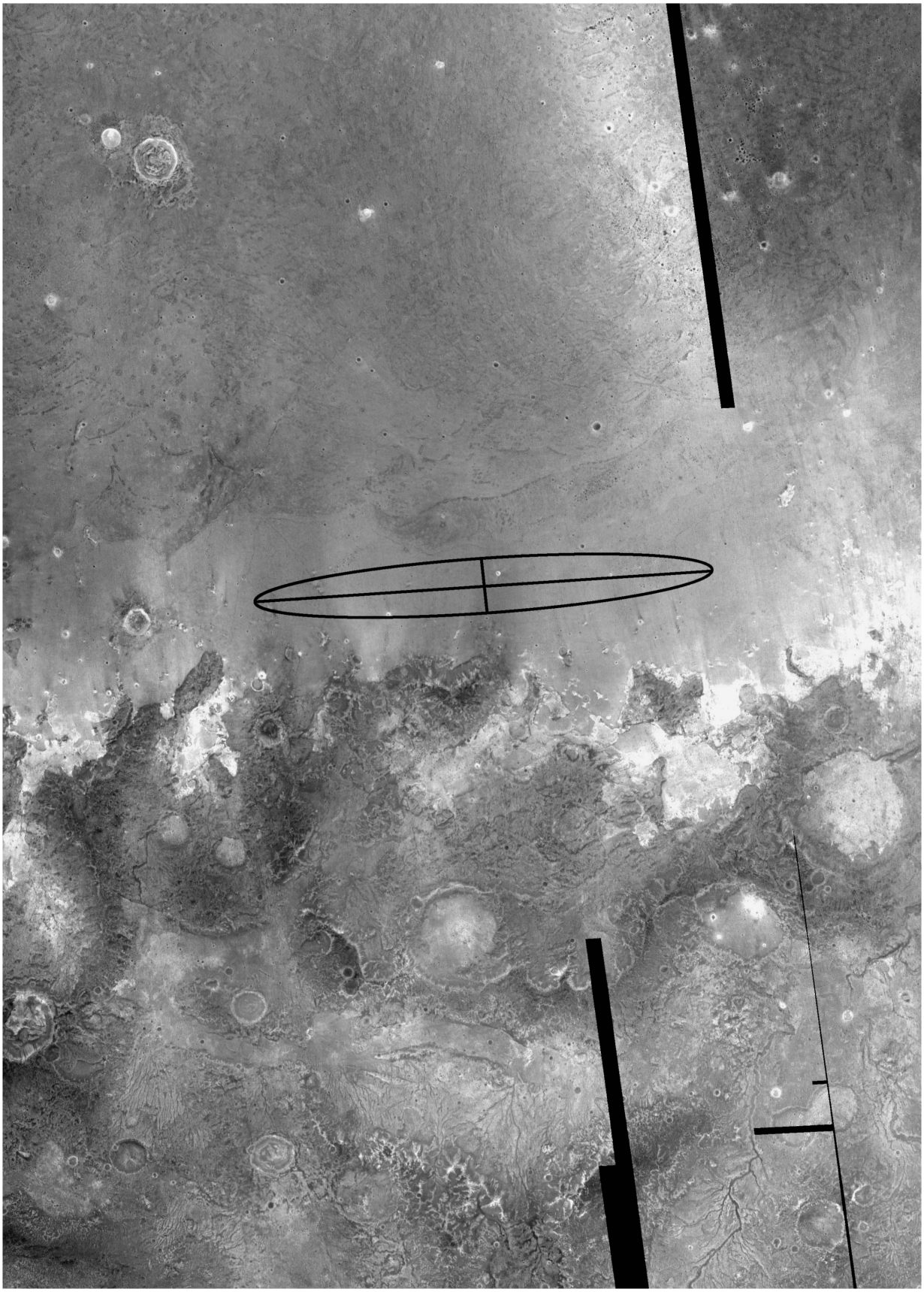

Fig. 15. A mosaic of THEMIS band 9 nighttime IR temperature data covering the region of the Isidis Planitia basin landing site. The mosaic is centered at 3.93° N, 88.0° E. The intended landing ellipse is shown in black and has a semi-major and semi-minor axis of 135 and 16 km, respectively.

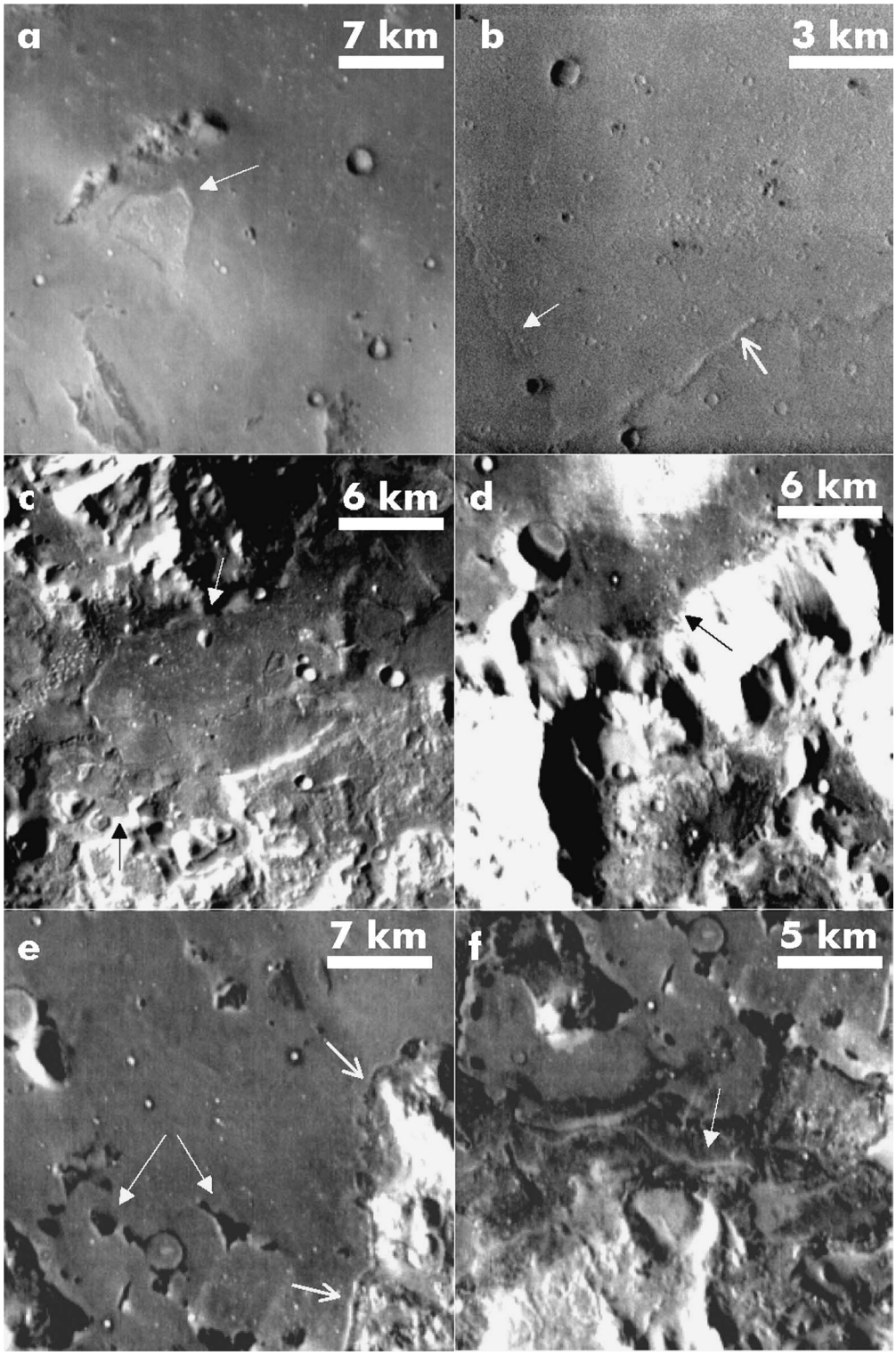

Fig. 16. THEMIS daytime IR temperature images (a), (c)–(f), and THEMIS VIS image (b), showing examples of features on the floor and rim of the Isidis Planitia basin that are interpreted to be volcanic in origin. (a) Arrow points to a rimless depression. This may be a result of collapse due to subsidence. (b) Solid arrow points to a small channel on the basin floor. This channel cannot be traced to the massif terrain. Open arrow points to a small wrinkle ridge. This ridge can be traced in an east–west direction and is oriented roughly parallel to the basin margin. (c) Possible flow fronts that contact the degraded massif terrain. This area is in the transition zone between the massif terrain and the basin floor. (d) Contact between basin floor material and massif. The basin floor material appears to superimpose the massif. (e) Solid arrows point to embayment relationships of basin floor material with cooler material. Open arrows point to a terrace around the northern base of the massif. Terraces found in lunar maria are attributed to subsidence of the maria surface. (f) Small axial channel found in cool surface material near the rim-basin boundary. These are characteristic of collapsed lava tubes found in intact lava flows (e.g., Basaltic Volcanism Study Project, 1981, p. 711).

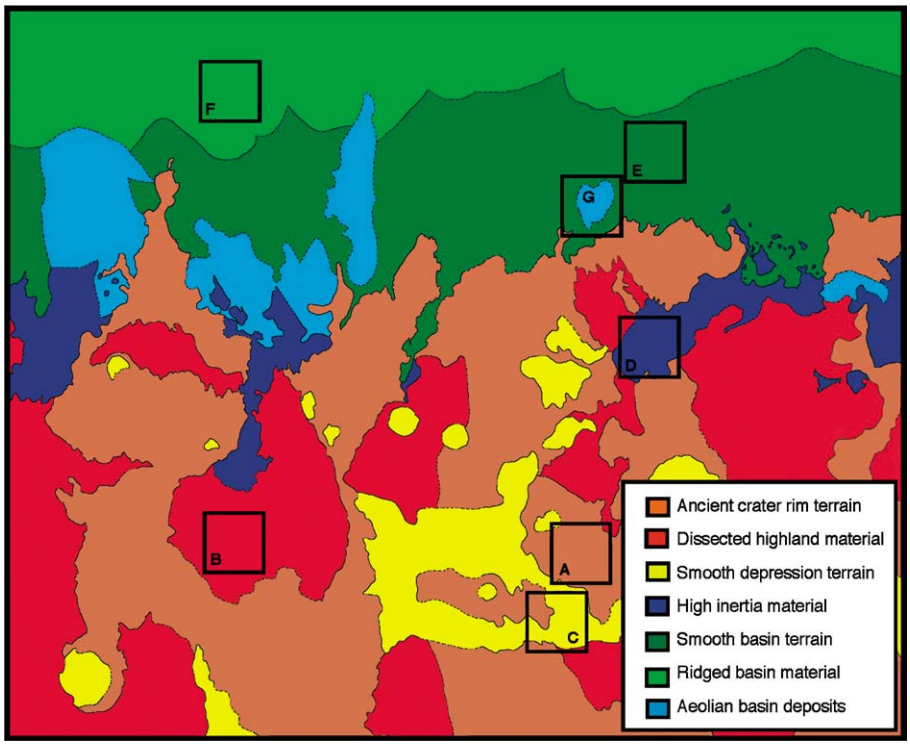

Fig. 17. Surface unit map of the Isidis Planitia basin rim and floor extending from 5.4° N, 84.7° E to 1.5° N, 89.2° E. (Note: different coverage than Figs. 14 and 15.) Boxes designate type example locations from Fig. 18. Units have been identified based on their thermophysical and morphological characteristics.

Viking images, are found throughout the rim area. However, the increased spatial resolution of THEMIS data reveals that these drainages are more abundant than previously observed. No channels observed in this region can be traced to the landing ellipse or the basin floor.

Landforms of interest on the basin floor include rimless depressions, terraces, possible kipukas (islands surrounded by lava), small-scale (200–300 m wide) wrinkle ridges (these are distinct from the large-scale ridges observed in MOLA data), and small, linear depressions (<200 m wide) that vary in sinuosity (Fig. 16). These features also are common in lunar maria (Guest and Greeley, 1977; Basaltic Volcanism Study Project, 1981, p. 758) suggesting a possible analog for the Isidis basin floor.

Comparison of the daytime and nighttime mosaics (Figs. 14 and 15) shows regions along the rim boundary that are warmer than their surroundings both during the day and night. This diurnal thermal signature probably is from coarse material with a low-albedo. These regions approach the southern border of the landing ellipse and correspond with TES-derived thermal inertias of 500 to ~800. There also are regions that are warmer during the night but cooler during the day. Relative to the surroundings, these regions have a higher albedo. This combination of relatively high albedo, cooler daytime, and warmer nighttime temperatures constrains the surface to be more coarse-grained or rockier than the surrounding terrain, but with a thicker dust mantle than other units. Within the landing ellipse, the infrared daytime and nighttime images illustrate that the thermophysical properties are relatively uniform; neither thermal inertia nor albedo vary significantly. Finally, it is worth noting that there is a lack of thermophysical signatures present on the basin floor that might be expected for near-surface fluvial deposits, such as fan-shaped accumulations of coarse-grained or rocky material.

2.3.2. *Surface units identified from THEMIS data*

Seven different surface units are readily distinguishable in the THEMIS mosaics based on thermophysical and morphological characteristics. These surface units, in order of apparent age from oldest to youngest, are: (A) highland massifs, (B) dissected highland material, (C) smooth highland depressions, (D) high inertia material, (E) smooth basin terrain, (F) ridged basin material, and (G) aeolian streaks. Figure 17 illustrates where these units typically occur in the study region, and Fig. 18 provides type examples of each unit.

Units A, B, and C. Three units have been identified within the highland terrain. The massifs (A), dissected surfaces (B), and smooth depressions (C) all have similar albedo (~0.21–0.24) and thermal inertia (~150–350). It is likely that these three units all are mantled by a thin dust layer based on the narrow and relatively high albedo values along with a DCI index in the range of ~0.94–0.96, which is intermediate between dust-covered and dust-free surfaces respectively (Ruff and Christensen, 2002). The massif Unit A is interpreted to be remnant crater rim material left over from the

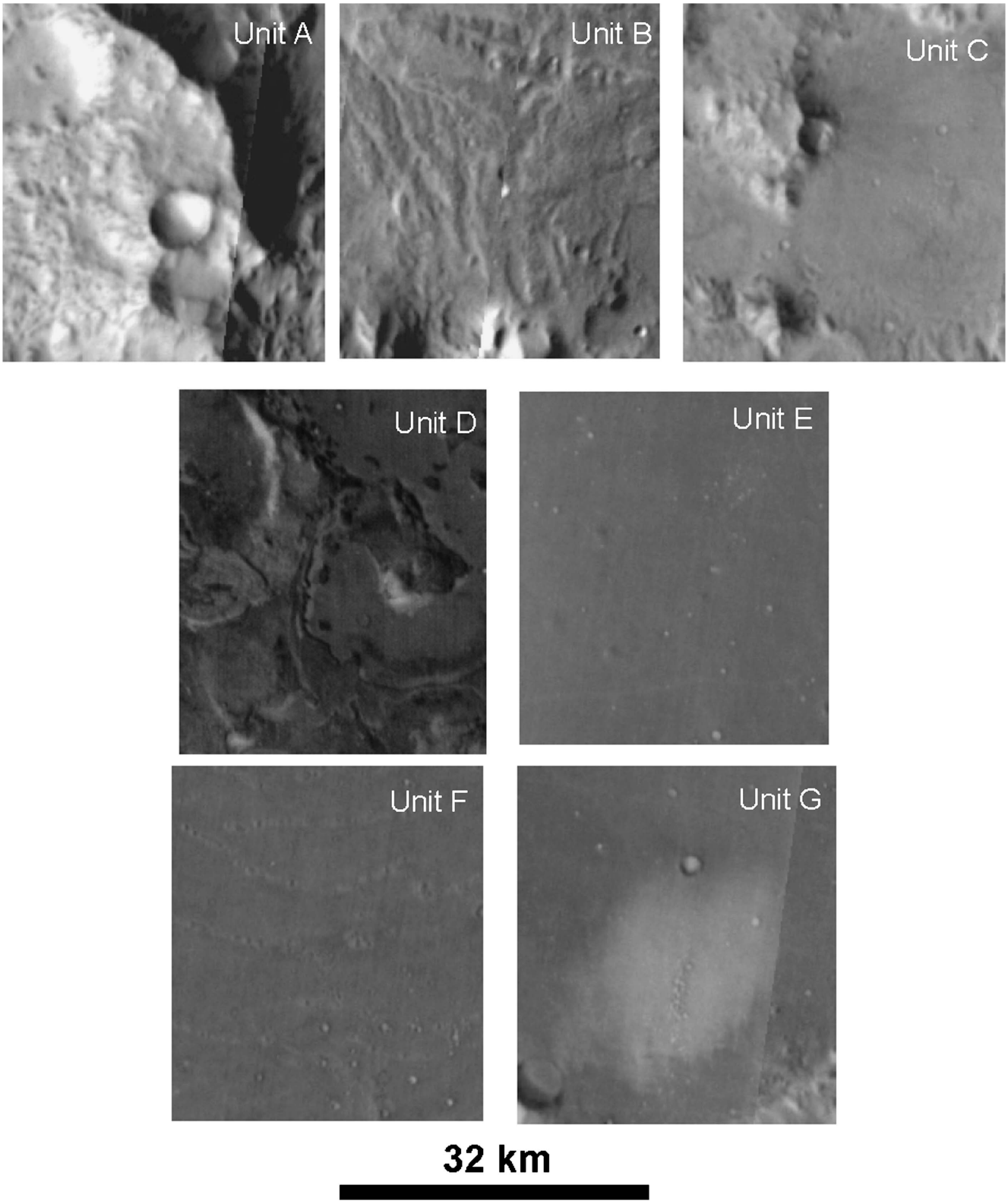

Fig. 18. Type examples for each of the mapped units in Fig. 17: Unit A highland massifs; Unit B dissected rim material; Unit C smooth material associated with large depressions in the rim terrain; Unit D higher inertia material at the rim-basin boundary; Unit E smooth basin material; Unit F basin material containing ridges; and Unit G variable aeolian features within the basin.

period of heavy bombardment and the Isidis Basin impact event (Greeley and Guest, 1987). This unit occurs as topographically high features in the form of ridges and mesas representing ancient crater rims that have undergone sig-

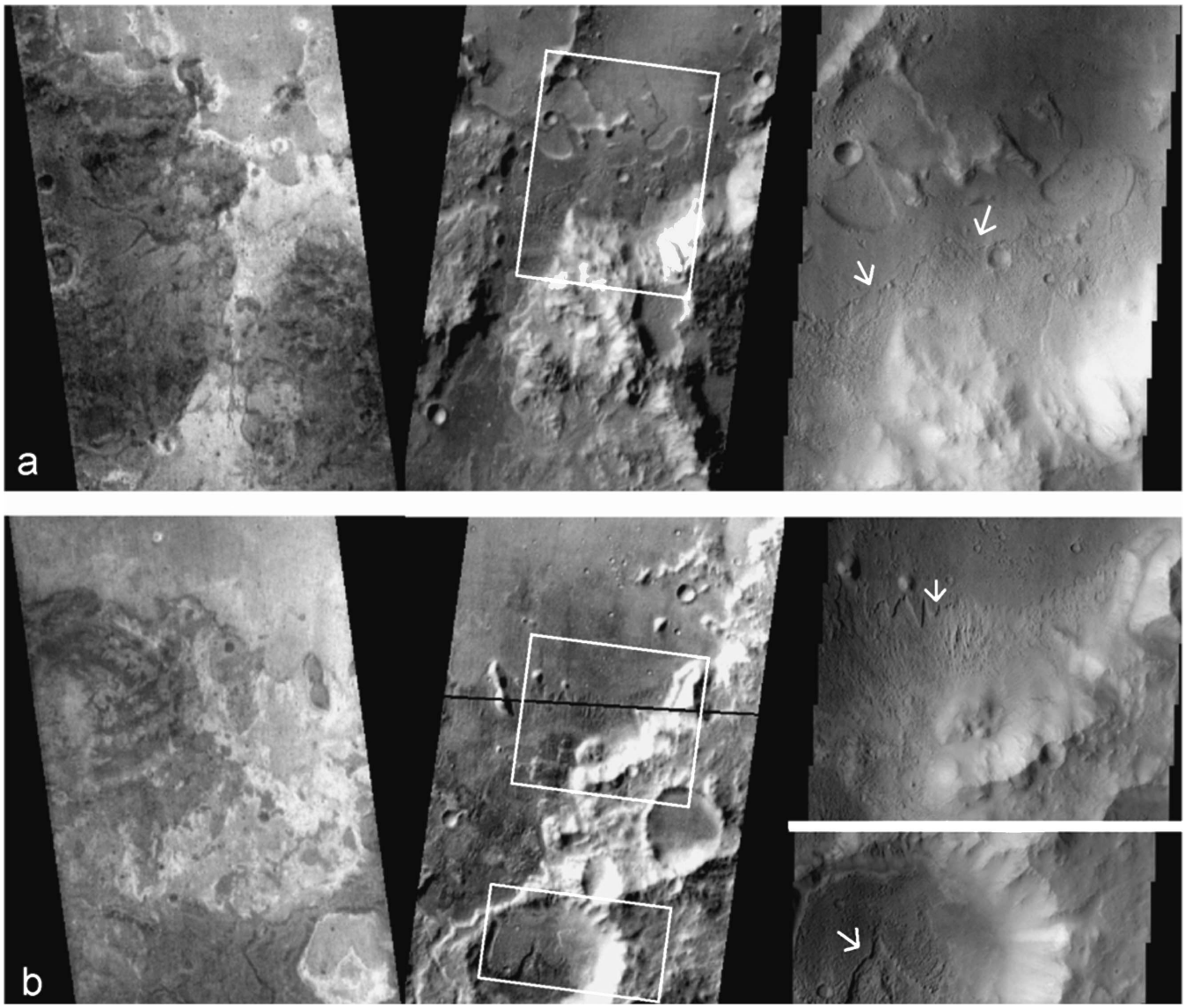

Fig. 19. THEMIS nighttime and daytime IR and VIS images of the Isidis rim (left to right) over 2 areas (a), (b) within the high-inertia unit. For scale, the width of the nighttime and daytime images is ∼32 km; the width of the VIS images is ∼19 km. Locations of VIS images are indicated by white boxes in the daytime IR images. (a) Partial THEMIS images I02987003, I03180005, and V03180006. Arrows point to contacts between the smooth and rough material within Unit D, the higher inertia material. (b) Partial THEMIS images I05284005, I03205002 (the black line across the center represents missing data), and V03205003. Arrows point to the contact between the smooth and rough material within Unit D. In both examples, it is clear that the smooth material is overlying the rough material. In (b), the smooth material appears to have been eroded to expose the rough material beneath.

nificant modification by erosion. The dissected channels of Unit B are observed solely amidst the highland massifs. These channels occur at the same topographic level, either outside crater rims, or inside craters, implying a sapping or ground water origin (Carr, 1996). The channels are uniform in size and all are terminated by either the smooth depression terrain (C) or highland massifs (A). There is no evidence that these channels are currently active or recently have deposited material into the Isidis basin. Finally, the smooth depression terrain (C) is characterized by relatively featureless surfaces forming linear depressions that branch around topographic obstacles. Fewer craters are observed in Unit C than the other two, suggesting a younger surface. The smooth depressions contain features that resemble lava flow fronts, indicating a volcanic rather than fluvial origin.

Unit D. The high inertia unit is observed only in small patches within topographic breaks at the basin-rim boundary. Relative to its surroundings, this material has a cooler temperature during the day and is the warmest surface at night. This indicates a higher thermal inertia (the highest in this region ranges from 600 to 715 from TES data) and possibly a coarser particle size than the smooth basin terrain (E) and the ridged basin material (F). The edges of Unit D commonly are defined by lobate scarps. Figure 19 illustrates

that at least 2 different surface textures are apparent within the high inertia unit. These generally can be described as "smooth" and "rough" with the smooth material lying topographically above the rough material. The surface texture of the smooth material resembles that of the smooth basin terrain (E) while the rough material has an etched appearance. Figure 19 highlights two different regions within the high inertia Unit D where the contact between the smooth and rough material is observed. In one example, the edge of smooth material is jagged, suggesting that this terrain has been eroded away to expose the underlying rough material.

It is difficult to determine unequivocally the origin of the high inertia unit. There are conflicting observations demonstrating that the material composing the high inertia unit may have originated from either the highlands or from the basin. However, it is clear that this unit has undergone, and is probably currently experiencing, a significant amount of erosion. The location of the high inertia unit within topographic lows at the rim-basin boundary likely contributes to the efficiency of dust-removal in these areas with winds being channeled through the lows. Unit D, the highest inertia material in the whole scene, is confined to regions near the massif boundary and is not found within the landing ellipse.

The lobate scarps found within Unit D are characteristic of mass wasting processes (Tanaka, 1997; Tanaka et al., 2003), and suggest that Unit E and the landing ellipse area could consist of material eroded from Unit D. However, this hypothesis is considered less likely because: (a) there is no evidence for flow direction within Unit E, (b) Unit E completely embays Unit D in some areas (see Figs. 16 and 17), (c) lobate scarps are also found within Unit E, and (d) there is no thermophysical variation within Unit E that would be characteristic of debris aprons. It is possible, however, that materials derived from mass wasting of Unit D could have been buried by Unit E.

Units E and F. The smooth basin terrain (E), which hosts the landing ellipse, has little variation in either morphologic characteristics or thermophysical properties (thermal inertia of 350 to 550; albedo of 0.22 to 0.23). The southern margin of Unit E appears to embay highland material, as also noted by Tanaka et al. (2003), who mapped Unit E as boundary plains unit 2. The northern boundary of the smooth basin terrain is marked by a ∼1 K decrease in daytime surface temperature. The origin of this temperature "contact" is uncertain, but the simplest explanation is that fine particles are more easily trapped on the northern side of the contact. This preferential trapping may be due to a difference in surface texture. It is interesting to note that this contact corresponds to the southern margin of the Vastitas Borealis Formation (VBF) (Scott et al., 1987; Tanaka et al., 2003) and to Contact 2 of Parker et al. (1989, 1993). Tanaka et al. (2003) interpret the VBF in this region as material that was extensively reworked by permafrost- and mass wasting-related processes during the late Hesperian to early Amazonian. Perhaps the suggested difference in surface texture is related to the modification processes that formed the VBF. The ridged basin material (F) has similar thermophysical properties as the smooth basin terrain and is characterized by small (∼500 m wide), ridge-like features with depressions at their summits. Interpretations for the origin of these features includes fissure vents associated with volcanic activity (Carr, 1981), pseudocraters (Frey and Jarosewich, 1982), cinder cones (Plescia, 1980) mud volcanoes (Tanaka, 1997), or glacial features (Lucchitta, 1982; Grizzaffi and Schultz, 1989).

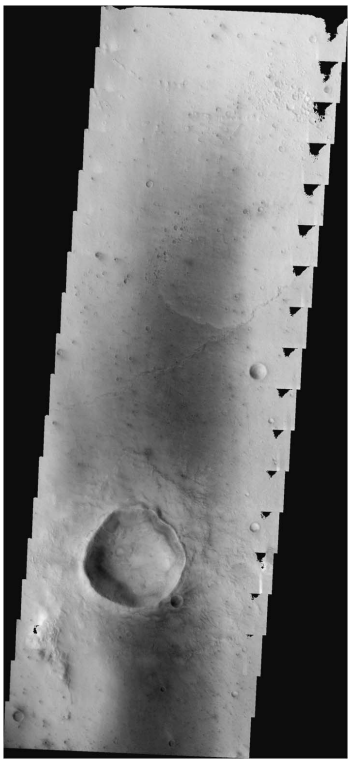

Fig. 20. THEMIS VIS image V01008005 showing an apparent wind streak on the floor of Isidis basin (image width ∼19 km).

Unit G. On the basin floor W and S of the ellipse are wispy streaks that are warmer by several degrees than the floor in the daytime IR mosaic (Fig. 14) that show only a vague counterpart in the nighttime scene. These streaks correspond to relatively low albedo features evident in visible wavelength images (Fig. 20). They typically occur on the basin floor adjacent to topographic lows in the highland terrain. The lack of a clear counterpart of the streaks in the nighttime mosaic suggests that these visibly dark features are the result of removal by wind of a thin dust layer revealing a darker substrate. Because the dust layer is thin, removing it does not lead to a significant change in thermal inertia.

2.3.3. Channel mapping with THEMIS data

The unit map (Fig. 17) demonstrates that the dissected surfaces within the rim terrain do not come into contact with the basin floor. In an effort to determine the extent of small channels on the basin floor, a combination of THEMIS VIS

and daytime IR images were examined. Thin (1–2 pixels wide) linear features can be traced in daytime IR images. However, in areas that lack supplementary high-resolution visible images, it is difficult to discern whether these features are channels (negative relief) or ridges (positive relief). Only a few small channels on the basin floor come into contact with the rim terrain; however, there are no rim terrain channels that link to basin floor channels. Other small basin-floor channels end or taper out before reaching the rim terrain. Increased coverage with the VIS camera will help clarify the extent of the small channels, but our preliminary analysis finds no connection between the channels found in the basin and the dissected material observed in the rim terrain. It is therefore probable that the small channels and dissected terrain are unrelated, and formed by different mechanisms, possibly during different time periods.

2.3.4. Discussion

Beginning with observations from the Viking IRTM, elevated thermal inertia values have been observed along the southern rim of the Isidis basin (Palluconi and Kieffer, 1981). The presence of this relatively high inertia region along the transition between basin rim and floor recently has been included in the hypothesis that ancient highland materials have been delivered to the basin floor (Golombek et al., 2003). A critical assessment of this hypothesis is now possible with a combination of data sets. Figure 21 shows TES-derived thermal inertia at full spatial resolution superimposed on a MOLA shaded relief map to illustrate where thermophysical variations occur in relation to landform expressions. In this presentation, only values of thermal inertia $\geqslant$350 are shown in an effort to highlight those areas that have significantly elevated values. The full TES data set was used without filtering for season in an effort to achieve the maximum spatial coverage. This has produced a marked streakiness in the thermal inertia overlay that is attributable to variations in atmospheric conditions with season that are not accounted for in the derivation of thermal inertia values. Nevertheless, a clear pattern of elevated values is evident along the rim margin.

The highest thermal inertia values shown in Fig. 21 are concentrated amidst the highland massifs and correlate well with locations identified in THEMIS images as Unit D. The morphology of Unit D suggests an in-place geologic unit that possibly has been exposed by aeolian erosion. The lower range of thermal inertia values extends as much as 250 km out onto the basin floor. There are no apparent discrete boundaries or contacts that define the basin-floor expression of elevated thermal inertia values. Instead there appears to be a general decrease in thermal inertia away from the basin rim terrain.

Albedo patterns evident in Viking and MOC images along the Isidis rim provide additional clues about the origin of the elevated thermal inertia signature (Fig. 22). The dark-toned streaks extending from the rim onto the floor of the basin appear to be oriented in a direction that suggests that basin directed winds have been active along the pronounced topographic divide and perhaps are funneled by breaks in

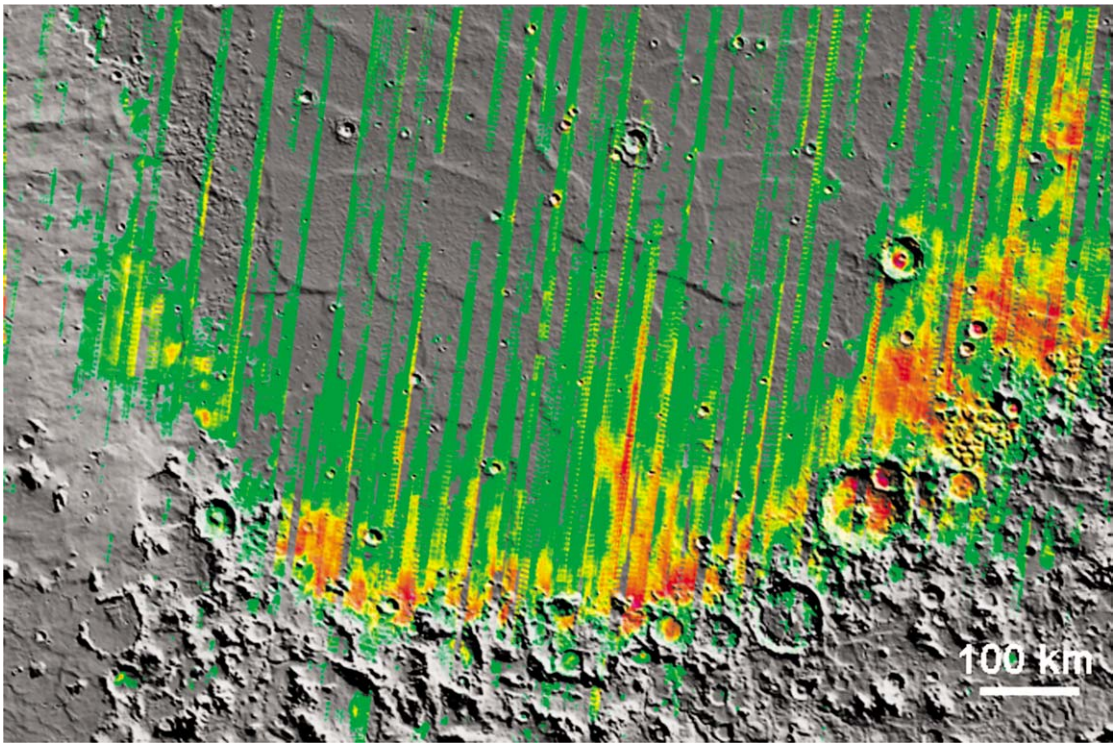

Fig. 21. TES-derived thermal inertia data at full spatial resolution overlain on MOLA shaded relief data of Isidis Planitia centered at 8.1° N, 87.7° E. Colors represent values ranging from 350 to 700 $\mathrm{J\,m^{-2}\,s^{1/2}\,K^{-1}}$ (green to red hues).

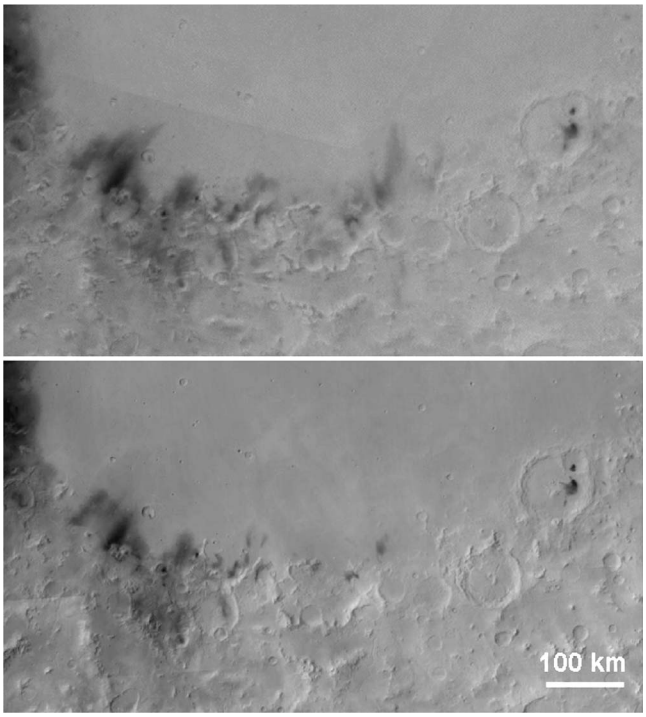

Fig. 22. Viking MDIM (upper frame) and MOC wide-angle (lower frame) mosaics of the Isidis Planitia rim centered at 4.1° N, 88.2° E showing basin-directed dark-toned streaks. These may be produced from winds funneled through breaks in topography. Such winds could produce a winnowing effect that leads to a coarser lag deposit and thus an elevated thermal inertia signature like that seen in Fig. 21.

the topography. The dark-toned streaks are diminished in the MOC wide-angle mosaic relative to the Viking mosaic, suggesting a net accumulation of dust in recent times (Fig. 22). Based on TES albedo and DCI values, much of the basin rim and floor is covered by a layer of dust that is thick enough to be observable in these measurements but thin enough not to obscure the thermal inertia signatures. This layer would be on the order of 10s of microns to a few millimeters thick. Such a layer of dust could be removed by wind-blown saltating particles to reveal a darker substrate, creating the streaks that are observed. Over time, this wind activity could lead to a winnowing of the finest particles at the surface to produce a coarser lag. This would be evident as an elevated thermal inertia signature. The decrease in thermal inertia with distance from the rim also is consistent with a wind-winnowing scenario. The 10s to 100s of kilometers over which the elevated thermal inertia signature is observed is better reconciled by an aeolian process rather than by fluvial transport. It is unlikely that the very low topographic gradient of the basin floor could support the transport of highland material to such distances by putative runoff from the rim.

2.3.5. Implications and predictions for the proposed landing site

The intermediate spatial resolution and IR imaging capabilities of THEMIS allows for more informed predictions of what the rover would observe at the landing site. The site was proposed as an opportunity to sample ancient highland material deposited in a fluvial environment. Current THEMIS coverage illustrates that drainages and channels within the ancient highland terrain do not reach the basin floor, and small channels on the basin floor cannot be traced to the highlands. Although elevated thermal inertia regions are present along the basin-rim margin, these likely are due to aeolian reworking of the surface. Any materials that might have been deposited during the dissection of the rim terrain or by mass wasting of Unit D most likely are buried by later volcanic infilling events. Taken together, these observations diminish the likelihood of finding highland material in the landing ellipse.

2.4. Melas Chasma

Melas Chasma, a rugged canyon region in the central part of Valles Marineris, contains various interior deposits and other features whose origin in some cases remains enigmatic. There have been multiple hypotheses on the formation of the interior deposits by landslide, aeolian, alluvial, lacustrine, and volcanic activity (Sharp, 1973; Lucchitta, 1987; Nedell et al., 1987; Komatsu et al., 1993; Peulvast and Masson, 1993; Lucchitta et al., 1994; Malin and Edgett, 2000), but there is yet no consensus. Recent analysis of MOC images of the landing ellipse region has revealed an unusual terrain consisting of rounded or ovoid blocks that appear lighter-toned than their surroundings (Skilling et al., 2002; Weitz et al., 2003). They have long-axis dimensions ranging from <100 m to 1 km (Skilling et al., 2002) and commonly are surrounded by light-toned aeolian bedforms. The origin of the blocky terrain remains uncertain but emplacement by mass movement processes is a favored explanation (Skilling et al., 2002; Weitz et al., 2003). Also evident in MOC images are regions covered by dark-toned sand sheets and dunes (Weitz et al., 2003).

Melas Chasma was suggested as a potential landing site because of its intriguing nature and scientific potential. The site made it to a short list of four primary sites but was then eliminated based on models of high winds within the canyon (Kass et al., 2003; Rafkin and Michaels, 2003) and excessive roughness within the ellipse (Kirk et al., 2003). The specific region examined in this study includes both floor and wall material as shown by the Viking MDIM2 and geologic map of Scott and Tanaka (1986) and expanded upon by Pelkey et al. (2003). Floor elevations r ange from −4446 to −3090 m while elevations on the canyon wall reach 1130 m. Three generalized geomorphic units are present on the floor: (1) landslide deposits; (2) the blocky unit; and (3) dunes and sand sheets. Albedo in this area ranges from ∼0.12–0.20 while DCI values range from 0.95–0.98. These values are indicative of surfaces that range from partially or thinly dust-covered to dust-free (Ruff and Christensen, 2002). Thermal inertia derived from TES data ranges from ∼160–600 indicating that the surface structure at the decimeter scale varies significantly across the area.

2.4.1. THEMIS daytime IR

Although the complex topography of the canyon walls is the most noticeable feature of the daytime IR mosaic (Fig. 23), the western third of the canyon interior appears to be dominated by landslides. There are large, rugged landslides from the northern wall that extend onto the canyon floor as well as more subtle, multiple intersecting landslides with features resembling those noted by Witbeck et al. (1991). The latter type consists of vast aprons of material marked by concentric or longitudinal ridges and troughs that probably are created by compressional or differential flow respectively. It is possible that these flows were achieved by gas or water fluidization (Witbeck et al., 1991). Daytime temperatures vary across the ridges and troughs of these landslides, probably as a result of both topographic variations at their surface and variations of the material itself.

A prominent feature of the central portion of the scene is a mottled, dark-toned region that represents relatively low temperature surfaces intermingled with smaller areas of slightly higher temperature. This area is adjacent to the

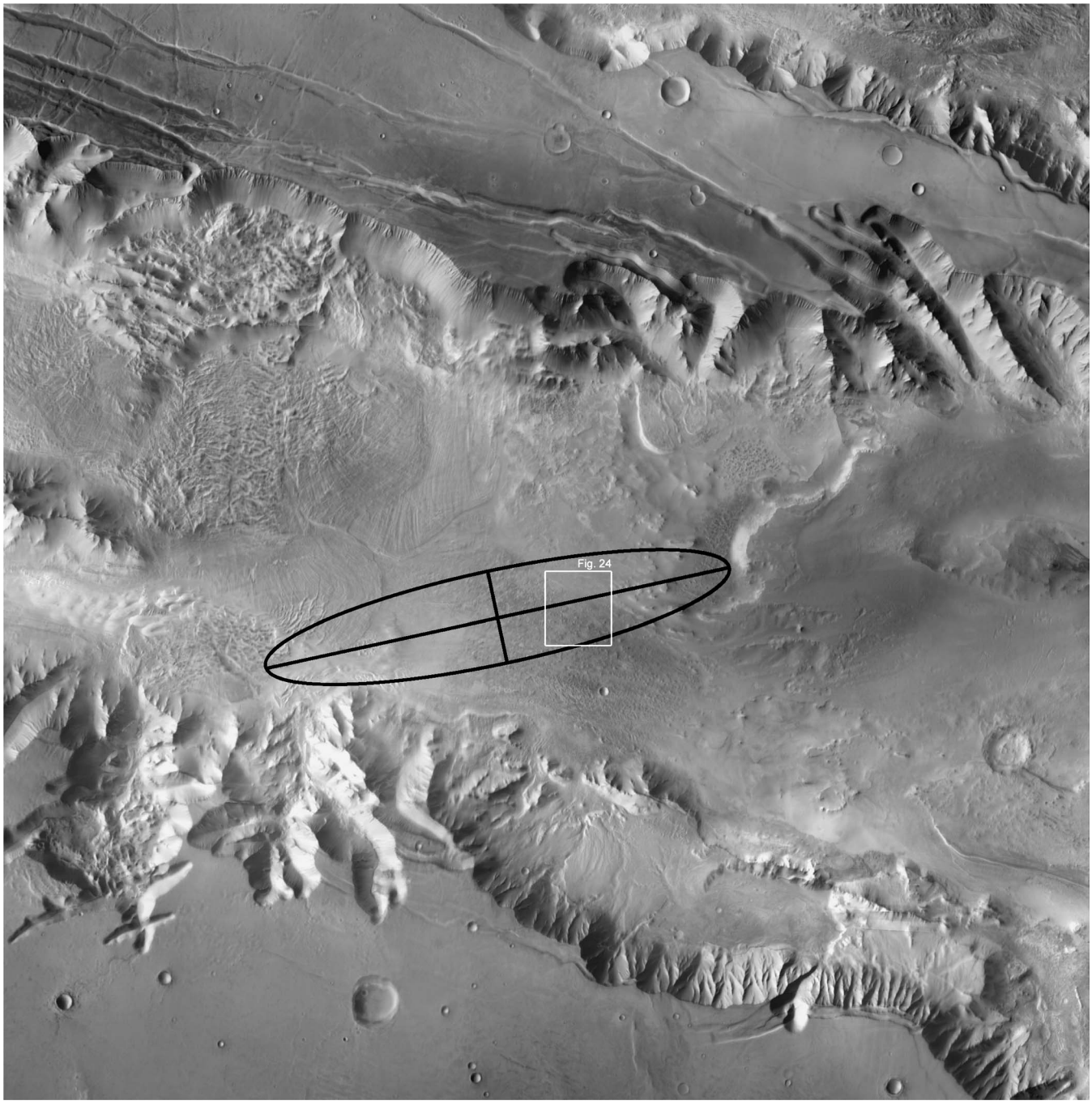

Fig. 23. A mosaic of THEMIS band 9 daytime IR temperature data covering the region of the Melas Chasma landing site. The mosaic is centered at 8.5° S, 282.8° E. The intended landing ellipse is shown in black and has a semi-major and semi-minor axis of 105 and 20 km, respectively.

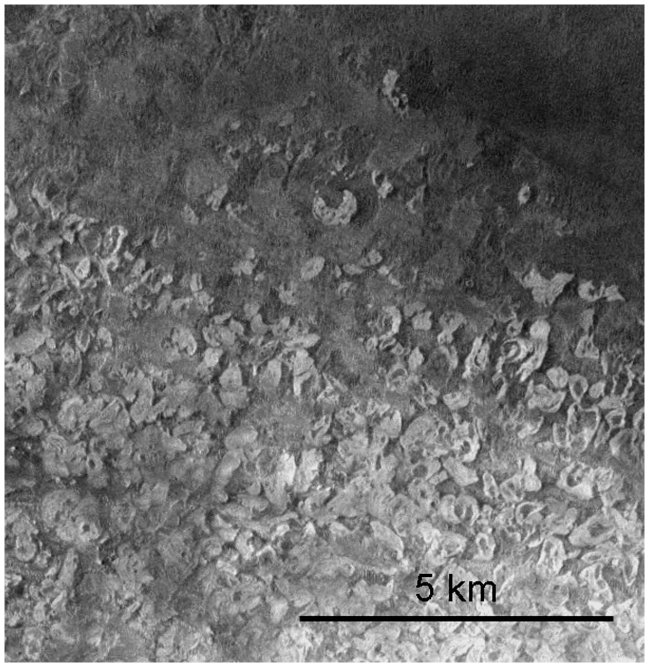

Fig. 24. A portion of THEMIS VIS image V01801002 centered at 8.7° S, 282.7° E showing the ovoid blocky terrain on the floor of Melas Chasma within the landing ellipse.

southern canyon wall extending ∼35 km into the canyon and is ∼60 km wide. As shown in THEMIS VIS (Fig. 24) and MOC images, this mottled terrain contains the unusual blocky unit described previously. The remaining floor areas host the dunes, sand sheets, and rippled terrain described in previous work (Pelkey and Jakosky, 2002). These areas appear relatively warm in the daytime IR mosaic.

2.4.2. THEMIS nighttime IR

Although slope effects are muted, the rugged canyon walls retain significant temperature variations at night (Fig. 25). The highest temperatures appear at the base of the walls and are fairly uniform across the lower elevations. Areas on the wall with more rugged topography show variations in temperature that range up to 15 K cooler than those at the base of the walls. A previous analysis by Pelkey and Jakosky (2002) suggested that particulate material could be covering portions of the canyon walls in layers that are perhaps ∼1–3 mm thick. It was also suggested that this layer thins downslope to reveal a rough, rocky surface at the base of the walls. The THEMIS observations generally support this idea.

Nighttime temperatures vary across the landslides in the western third of the canyon interior (Fig. 25) probably due to variations in the surface layer within the ridges and troughs. This scenario was hinted at in the daytime IR data, but it is difficult to separate slope-related temperature effects from those explicitly related to surface material properties. The temperatures across the landslides vary by ∼10 K. TES albedo of this area is quite low (∼0.130), indicating that the surface most likely is dust free. The thermal behavior suggests that the higher-temperature portions have a relatively high thermal inertia that may be due to exposed, indurated, or rocky material. The slightly cooler temperatures could be caused by particulate material that has become trapped in the troughs while the ridges remain exposed. TES thermal inertia values for these areas (∼300–400) are consistent with this scenario, but do not reflect the detailed structure seen in THEMIS images.

The central region that hosts the blocky terrain appears as two areas with relatively high nighttime temperatures intermingled with smaller areas of temperatures 15–20 K cooler (Fig. 26). Although the size of the blocks approaches the limit of THEMIS IR resolution, they are identifiable in THEMIS VIS images (Fig. 24). It is possible to correlate the blocks with the higher temperature surfaces within the unit, indicating a higher thermal inertia material. The cooler temperatures probably correspond to interspersed particulate material with a lower thermal inertia. The general boundary of the larger blocky terrain agrees well with a high thermal inertia area in TES data. In locations where the high-temperature deposits dominate the TES field of view, the derived thermal inertia values are ∼430–600 although sub-pixel spatial heterogeneity could result in the blocks having an even higher thermal inertia. Nonetheless, the higher-temperature surfaces of the blocks most likely are extensively indurated and/or contain rocky material. In locations toward the edge of this area where TES pixels probably are dominated by the lower-temperature dune material, derived thermal inertia values are ∼250–280. If we neglect sub-pixel mixing and assume that the dune material in these areas is simply loose, unconsolidated fines, the TES thermal inertia values correspond to particles ∼400–700 μm in diameter. These conclusions generally apply to the other smaller areas of blocky terrain as well, although the amount or size of the particulate material may vary.

The remaining areas are more uniform in the nighttime images. They represent the largest uninterrupted surfaces with the lowest temperatures on the canyon floor and generally correspond to areas with dunes, sand sheets, and aeolian bedforms. The large expanse of lower temperatures to the N and E of the central blocky unit corresponds to TES thermal inertias from ∼160–300. Pelkey and Jakosky (2002) concluded that the terrain in this area is covered by a thermally thick (> few cm) layer of particles ranging from 60–900 μm. The particles form small-scale ripples running in the cross-canyon direction like transverse dunes (Figueredo and Greeley, 2000; Pelkey and Jakosky, 2002) (Fig. 27). The ripples are not resolved in the THEMIS IR data but there is slightly more temperature heterogeneity in this area than was seen by TES, indicating that the coverage or thickness of the rippled material may be varying over the canyon floor.

2.5. Athabasca Valles

Remarkably well-preserved lava flows (Keszthelyi et al., 2000; Sakimoto et al., 2001; Plescia, 2003) and flood chan-

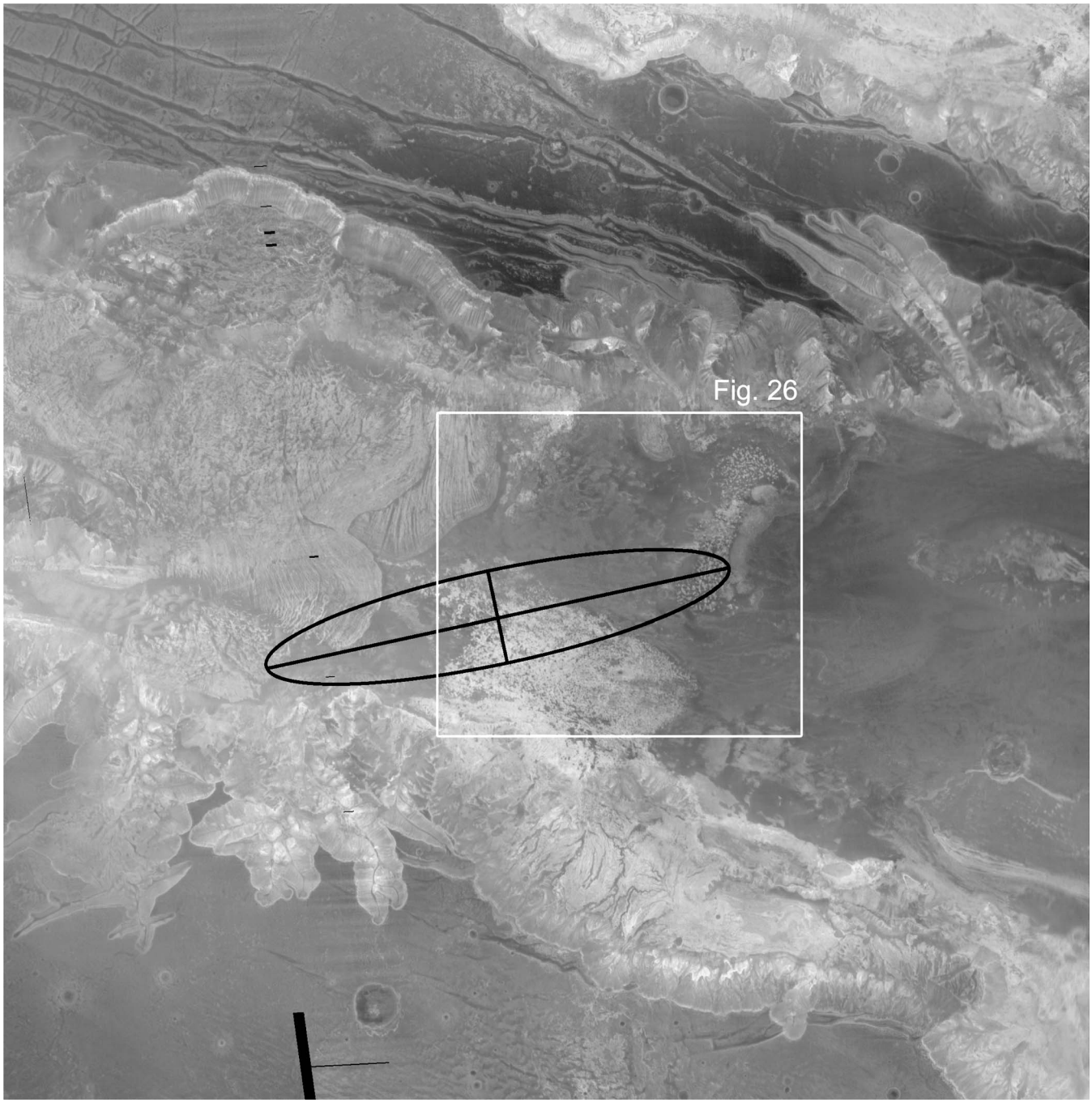

Fig. 25. A mosaic of THEMIS band 9 nighttime IR temperature data covering the region of the Melas Chasma landing site. The mosaic is centered at 8.5° S, 282.8° E. The intended landing ellipse is shown in black and has a semi-major and semi-minor axis of 105 and 20 km, respectively.

nels (Burr and McEwen, 2000; Burr et al., 2000) emanate from the Cerberus Fossae, a set of en echelon fissures trending E-SE from Elysium Mons. The distributary channels of Athabasca Valles (AV) contain the best-preserved examples of streamlined mesas, longitudinal lineations, terraces, and aqueous bedforms known on Mars. Such features can be interpreted as due to floods of water. Proximity to the source of these floodwaters was a key factor in the identification of AV as a desirable landing site. Materials brought up from the subsurface and deposited by the floodwaters would be targets of interest at this site. A concentration of streamlined mesas near the proposed landing site can be explained by a region of backwater that ponded behind ejecta from an impact crater in the channel (Burr, 2003). Further downstream to the southeast, the AV floodwaters may have ponded in a shallow depression covering 8.4×10^4 km^2, that was subsequently flooded by lava (Lanagan and McEwen, 2003). A small spillway and channels can be seen in THEMIS daytime IR images such as I02516009 near 3.9° N, 156° E. The Cerberus Plains to the south and west of AV are charac-

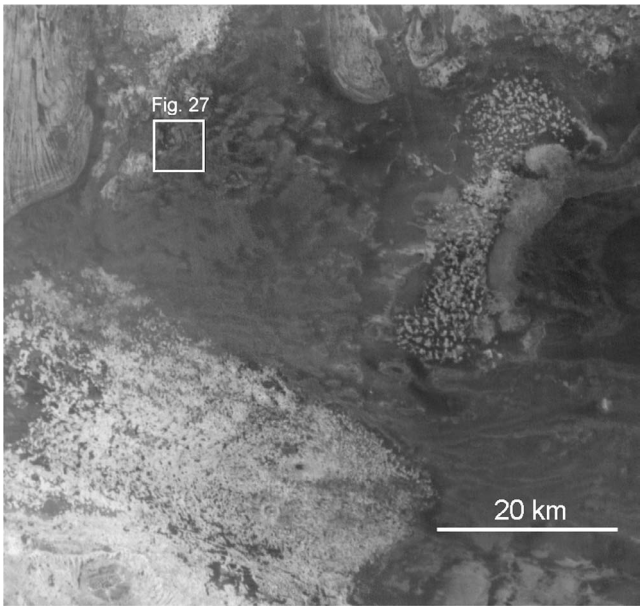

Fig. 26. An enlarged portion of the THEMIS nighttime IR mosaic of Fig. 25 centered at 8.6° S, 283.1° E showing the appearance of the blocky terrain on the floor of Melas Chasma in the lower left and upper right.

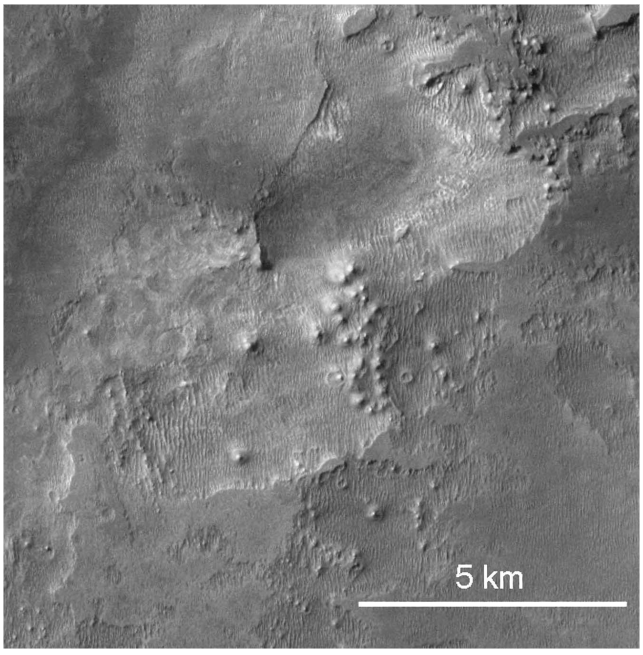

Fig. 27. A portion of THEMIS VIS image V03636003 centered at 8.3° S, 282.7° E from the central floor of Melas Chasma. The image shows small-scale ripples oriented in a cross-canyon direction that are interpreted as transverse dunes.

terized by a distinctive terrain with many ridges and rafted plates that can be reconstructed like a jigsaw puzzle. Previous workers have interpreted this platy/ridged terrain as lava (e.g., Keszthelyi et al., 2000; Sakimoto et al., 2001; Plescia, 2003). Apparent lava flows (some with plates and ridges) also are found in association with AV, but the relations have been unclear prior to THEMIS observations.

Eruptions of both water and lava from different portions of Cerberus Fossae have been described (Burr et al., 2000; Sakimoto et al., 2001; Plescia, 2003). However, the detailed relations between the volcanic and fluvial activity at AV, with implications for the source of water and geothermal activity, have not been clear. Viking Orbiter and MOC wide-angle cameras imaged the AV region at resolutions of a few hundred meters, but the images have low contrast due to the uniform albedo and low-relief topography. MOC Narrow-Angle (NA) images have proven very interesting because of the sharp, well-preserved morphologies at smaller scales, but cover only widely spaced slivers of the surface (except of the landing region that was considered for MER). MOLA has provided large-scale topographic data that revealed the largest channels of AV. Interpretation of the geologic history of this region has been hampered by the lack of useful regional-scale observations that enable extrapolation of the MOC results, a gap that is being filled by THEMIS.

2.5.1. *THEMIS IR*

The daytime and nighttime IR images (Figs. 28 and 29) of the AV region are remarkably similar with regard to the morphologic features that they highlight. Such similarity is due in part to the fact that albedo variations across the scene are small, precluding the daytime temperature variations that result from albedo contrast. TES data reveal a range of albedo values from ~0.23–0.29 excluding the fissures, which are too narrow to be fully resolved. This relatively narrow range of high albedo values likely is the result of a thin layer of dust covering the region, a conclusion supported by DCI values that include the range associated with partially to fully dust covered surfaces (0.91–0.95) (Ruff and Christensen, 2002). Additionally, the topography is relatively muted such that temperature variations due to slopes are minimized. Consequently, the temperature variations in the daytime IR mosaic of the AV region mostly result from thermal inertia variations. The fact that such variations are evident in the daytime and nighttime images indicates that the dust cover is thin, perhaps just a few millimeters.

Most of the temperature patterns closely correspond with morphologic units seen in overlapping MOC images, enabling extrapolation of unit maps over the entire region. Higher nighttime temperatures correspond to (1) rock outcrops in the steep slopes of fossae and craters, and (2) to very flat plains, often with well-expressed polygonal patterns. Lower nighttime temperatures correspond to bright-toned dunes and bright-rayed craters that probably have low thermal inertia (they are not resolved by TES). Platy/ridged lava in this region has high temperature contrasts (approaching 10 K) due to a lower-inertia cover over relatively high-standing plates separated by the higher-inertia polygonal ground (Fig. 30). Some lava flows also have clear temperature contrasts along their margins probably due to trapping of lower-inertia eolian materials (such as the bright dunes). Channel floors are generally intermediate in nighttime temperatures, but with streamlined patterns. All of the relatively

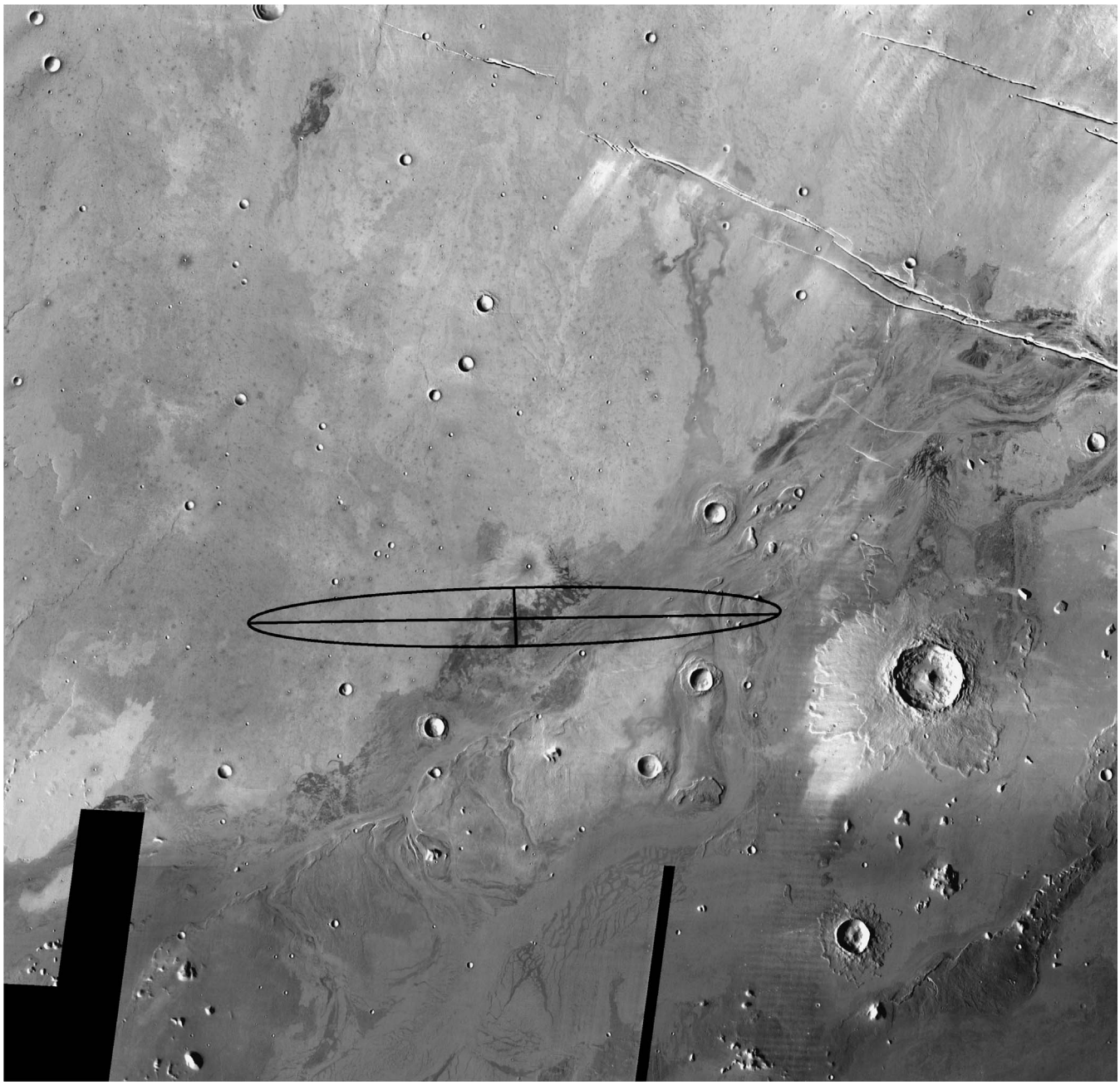

Fig. 28. A mosaic of THEMIS band 9 daytime IR temperature data covering the region of the Athabasca Valles landing site. The mosaic is centered at 9.2° S, 155.1° E. The intended landing ellipse is shown in black and has a semi-major and semi-minor axis of 152 and 16 km, respectively.

high-inertia polygonal ground appears to correspond to lava flows, which cover most of the floor of Athabasca Valles.

The fissures of Cerberus Fossae appear especially warm in the nighttime IR (Fig. 29) reaching temperatures >200 K, but we do not interpret this as evidence for geothermal anomalies. Given the apparently very young lava flows that erupted from the fissure system and the fact that the fissures are very sharp (i.e., reactivated), this would be a reasonable place to search for geothermal anomalies. However, it is highly unlikely that the entire fissure system could be geothermally heated, and there are good reasons to expect high nighttime temperatures from the passive thermophysics. The fossae are narrow (up to a few hundred meters) and have steep walls ∼100 m high that expose layers of lava, so it is expected to be relatively warm at night for two reasons: (1) the thermal inertia is probably higher, and (2) the sides and bottoms of the fissure radiate to much less than a full hemisphere of night sky. While there could exist geothermal anomalies in some spots along a fissure, the highest observed nighttime temperature within any of the fissures is 230 K. Such a temperature is consistent with exposed bedrock in the walls of a fissure. Much higher night-

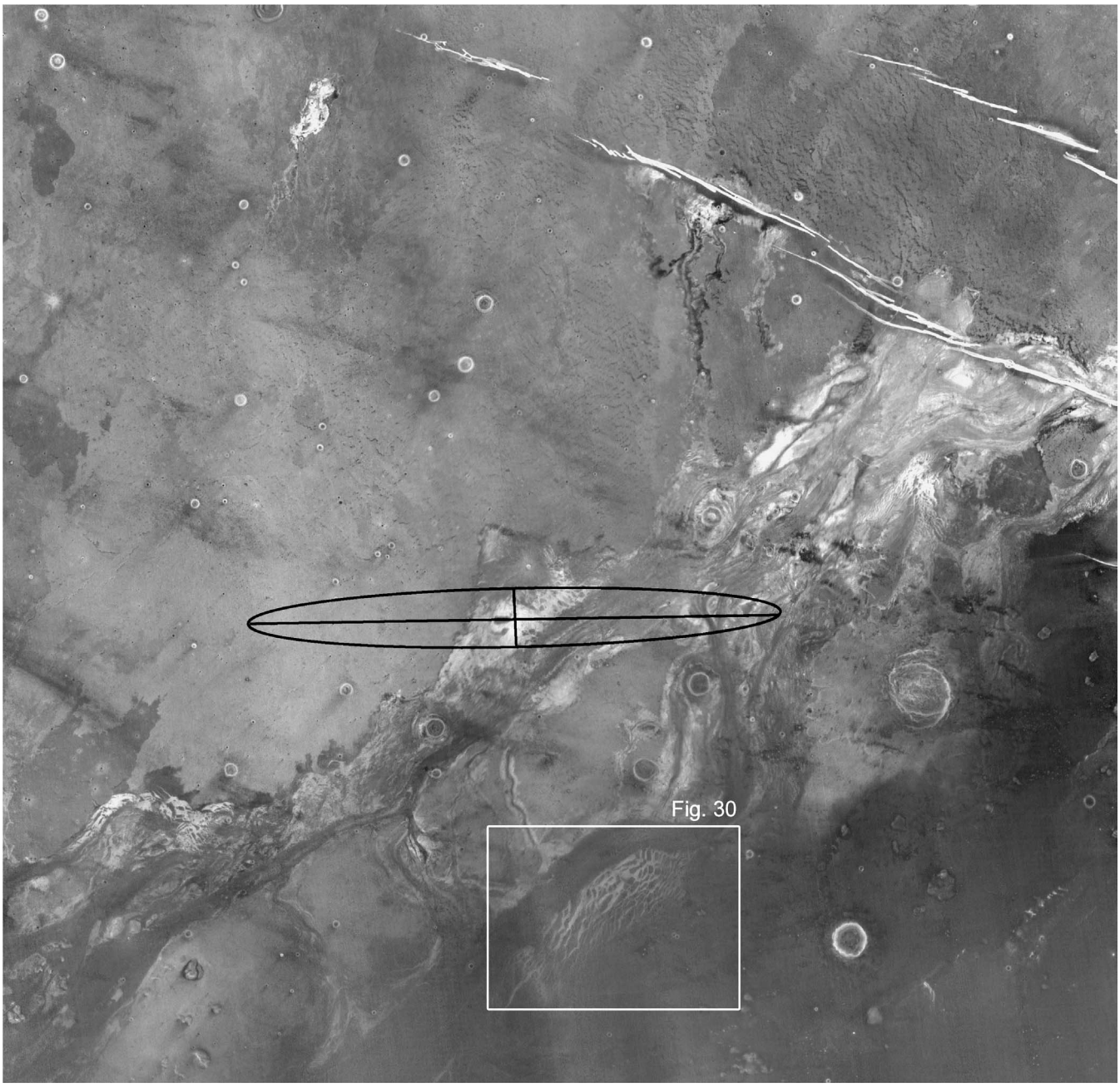

Fig. 29. A mosaic of THEMIS band 9 nighttime IR temperature data covering the region of the Athabasca Valles landing site. The mosaic is centered at 9.2° S, 155.1° E. The intended landing ellipse is shown in black and has a semi-major and semi-minor axis of 152 and 16 km, respectively.

time temperatures would have to be observed before a convincing case could be made for the existence of geothermal anomalies.

2.6. *Eos Chasma*

Eos Chasma lies at the eastern end of the Valles Marineris canyon system. The planned landing site lies within a smooth-floored, narrow portion of the canyon bounded by chaotic terrain to the east and west. This location is thought to have experienced catastrophic flooding throughout the Hesperian period from releases of huge volumes of subsurface water possibly related to the chaotic terrain in Capri and Eos Chasmata and outflow from Ganges Chasma to the north (e.g., Carr, 1981, 1996; Scott and Tanaka, 1986; Kuzmin et al., 2001; Greeley et al., 2003a). Evidence for flooding is found in the form of eroded channels on the adjacent plateau surfaces, terraces along the canyon walls, and oriented ridges and grooves on the floor.

While evidence for the passage of water through Eos Chasma is strong, it is unclear whether water persisted in this area. It has been suggested that a lake formed within the

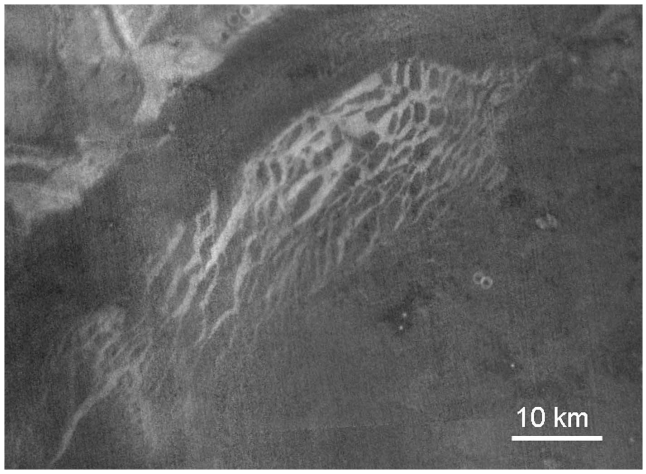

Fig. 30. An enlarged portion of the THEMIS nighttime IR mosaic of Fig. 29 centered at 7.4° N, 155.4° E showing the appearance of platy/ridged lava flows in the region of Athabasca Valles.

large collapsed depression of chaotic terrain to the west of the ellipse (Kuzmin et al., 2001; Greeley et al., 2003a). The interior layered deposits found within Ganges Chasma to the north are cited as evidence for standing water in that location (Carr, 1996). If these observations are correct, it is possible that the Eos Chasma site contains remnants of sedimentary material related to bodies of water more persistent than the ephemeral floodwaters. Such material would provide a partial rationale for landing at this location.

By all measures, this is a site with minimal dust accumulation. TES-derived thermal inertia values across the ellipse range from ∼500 to 700, albedo ranges from ∼0.13 to 0.17, and the DCI values of ∼0.96 to 0.98 fall within the range indicative of dust-free surfaces (Ruff and Christensen, 2002). These conditions would be optimal for in situ spectral measurements and would enhance the potential for relating such measurements to orbital observations.

2.6.1. THEMIS daytime IR

With nearly 5 km of relief and an abundance of topographic features, the daytime IR mosaic (Fig. 31) displays differential heating effects that highlight the geomorphology of the region. Canyon walls, chaotic terrain, and channeled surfaces for example, are observed with greater detail than provided by Viking images. While temperature variations related to topography dominate the scene, there are variations that arise independently of topography. Some of the small craters distributed across the canyon floor have cooler halos that appear to be related to ejecta and probably represent coarser material produced by impacts (Fig. 32). At the base of a segment of southern canyon wall with intense spur and gulley erosion, it appears that material has moved down slope and out onto the floor, producing a subtle distributary pattern observable as temperature variations (Fig. 32). Elsewhere on the floor, vague mottling is evident that indicates some heterogeneity in the particle size or induration of the floor materials.

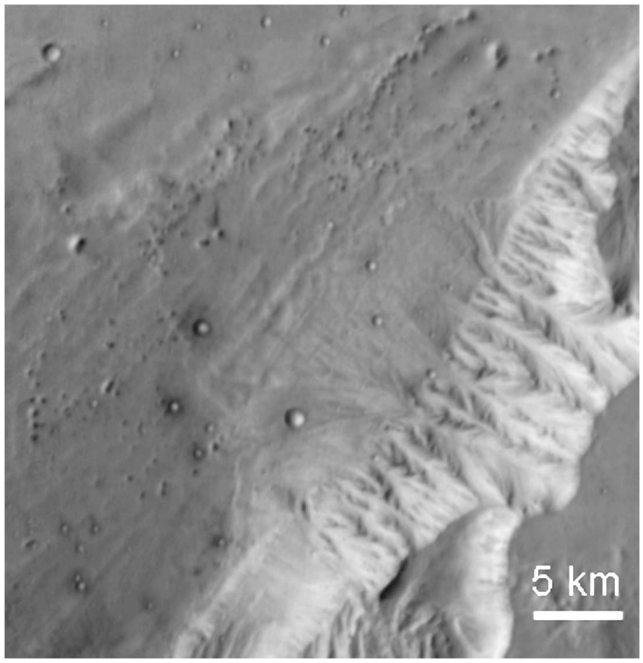

Fig. 32. An enlarged portion of the THEMIS daytime IR mosaic of Fig. 31 centered at 13.7° S, 318.5° E showing details of spur and gulley wall morphology and floor crater ejecta in Eos Chasma.

2.6.2. THEMIS nighttime IR

At night, a significant temperature contrast (>10 K) exists between the uppermost plateau surfaces and the canyon walls and floor (Fig. 33). Based on TES thermal inertia data, these upland surfaces have values between ∼270 and 350. This range is well above thermal inertia values associated with thick dust accumulation (< ∼125) but suggests that the plateau surfaces host finer-grained material than the canyon walls and floor. The canyon walls display most of the highest temperature features in the scene. Spur and gulley morphology is well resolved, with the ridgelines of the spurs commonly showing temperatures 10 K higher than the gullies (Fig. 34). This is consistent with the presence of coarser material on the spurs and finer material in the gullies. Figure 34 shows the same scene described in the previous section in which the apparent down-slope movement of material through the gullies has produced a distributary pattern on the canyon floor. Relative temperature differences are reversed in the nighttime scene, demonstrating that the lower temperature and presumably finer-grained material of the gullies fans out on the floor. Similar fans are evident on the northern wall of the canyon in the leftmost portion of the THEMIS daytime IR mosaic (Fig. 31) but not along its full length. This implies that spur-and-gulley style erosion has been active in some places following the floods that cut through the canyon.

The small craters on the canyon floor that appear with cooler halos in the daytime mosaic appear warmer than their surroundings at night (Fig. 34). The cool daytime/warm nighttime behavior of these craters almost certainly indi-

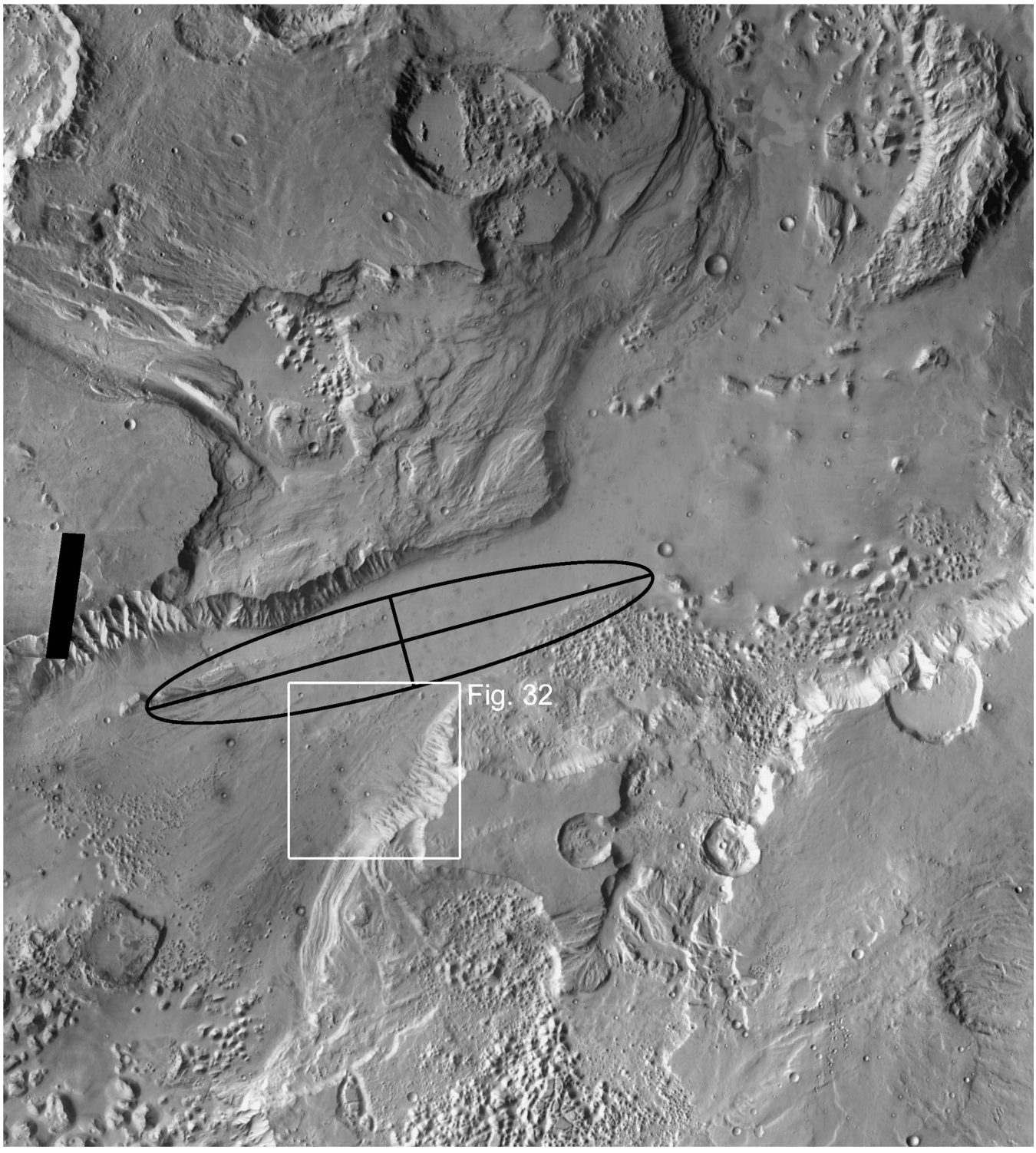

Fig. 31. A mosaic of THEMIS band 9 daytime IR temperature data covering the region of the Eos Chasma landing site. The mosaic is centered at 13.0° S, 319.0° E. The intended landing ellipse is shown in black and has a semi-major and semi-minor axis of 108 and 19 km, respectively.

cates a coarser material is present in the ejecta than on the surrounding floor. The fact that not all craters of similar diameter show this behavior likely indicates relative ages of the craters with those that show a thermal halo being younger than those that do not.

3. Summary

THEMIS images provide views of the MER landing sites that were not available until the end of the landing site selection process. In many cases, the combination of spatial

Fig. 33. A mosaic of THEMIS band 9 nighttime IR temperature data covering the region of the Eos Chasma landing site. The mosaic is centered at 13.0° S, 319.0° E. The intended landing ellipse is shown in black and has a semi-major and semi-minor axis of 108 and 19 km, respectively.

resolution, coverage, and SNR of the daytime IR images is superior to existing data sets, allowing new morphologic details to be observed. The nighttime IR images are most sensitive to variations in thermal inertia, thus supplying information about the nature of the martian surface layer at higher spatial resolution than previously available. As outlined below, the landing sites contain details that are presented more clearly with THEMIS observations.

1. In Meridiani Planum, the light-toned crater rims and mottled surfaces seen previously in MOC images appear to

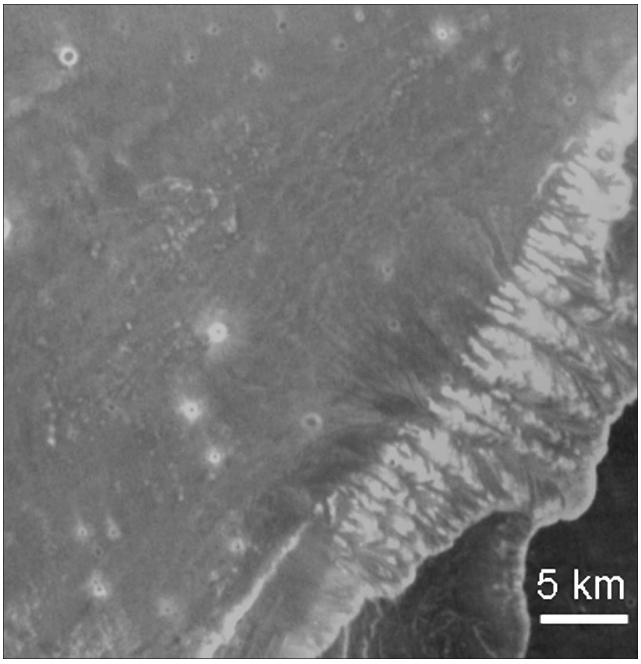

Fig. 34. An enlarged portion of the THEMIS nighttime IR mosaic of Fig. 33 centered at 13.7° S, 318.5° E showing details of spur and gulley wall morphology and floor crater ejecta in Eos Chasma.

be due to a higher inertia, visibly brighter unit just underneath the hematite-bearing layer.

2. In Gusev Crater, multiple units are present within the landing ellipse that display variations in thermal inertia and morphology that are indicative of a distinctive stratigraphic sequence that may be accessible to the rover.

3. The rim terrain of Isidis Planitia shows a greater density of channel networks than observed previously but no evidence that any channels empty onto the basin floor. The highest thermal inertia features are associated with a distinctive terrain confined to topographic lows at the rim/floor margin.

4. In Melas Chasma, the unusual, rounded blocky terrain seen previously in MOC images has an elevated thermal inertia signature that distinguishes it from the surrounding canyon floor terrains.

5. Although most of the Athabasca Valles region is covered by a thin layer of bright dust, both THEMIS daytime and nighttime IR images reveal a remarkable level of geomorphic detail, highlighting the different flows that have emerged from the Cerberus Fossae.

6. The presence of alluvial fans in at least two locations on the floor of Eos Chasma demonstrates that some spur-and-gulley erosion of the canyon walls has occurred following the floods that scoured the floor.

Acknowledgments

The THEMIS data set has been produced and refined to its current state through the hard work of mission planners and software developers. Thanks go to Kelly Bender, Laurel Cherednik, Kim Murray, Jayme Harris, and Andras Dombovari for their patience and dedication to acquiring this beautiful data set. Michael Weiss-Malik, Saadat Anwar, Ben Steinberg, Joel Hoff, and Randy Kaelber along with the ISIS programming group at the USGS in Flagstaff including James Torson, Kris Becker, and Debra Cook, have developed the essential software tools that allow us to achieve the results shown in this paper. Chris Edwards used these data and tools to create THEMIS mosaics of unprecedented quality. Of course none of this would have been possible without those who produced the THEMIS instrument at Raytheon Santa Barbara Remote Sensing. Constructive reviews by Ken Tanaka and Ashwin Vasavada served to improve the content of this paper. This work was supported by the NASA Mars Odyssey Project.

References

Arvidson, R.E., Deal, K.S., Hynek, B.M., Seelos IV, F.P., Snider, N.O., Mellon, M.T., Garvin, J.B., 2002. Thermal inertia, albedo, and MOLA-derived roughness for terrain in the Terra Meridiani area, Mars. Lunar Planet. Sci. XXXIII. Abstract 1748 [CD-ROM].

Arvidson, R.E., Seelos IV, F.P., Deal, K.S., Koeppen, W.C., Snider, N.O., Kieniewicz, J.M., Hynek, B.M., 2003. Mantled and exhumed terrains in Terra Meridiani, Mars. J. Geophys. Res. 108, 8073.

Basaltic Volcanism Study Project, 1981. Basaltic Volcanism on the Terrestrial Planets. Pergamon Press, New York.

Burr, D.M., 2003. Hydraulic modeling of Athabasca Vallis, Mars. J. Sci. Hydrol. 48, 655–664.

Burr, D.M., McEwen, A.S., 2000. Improved discharge calculations for the Cerberus region, Mars. Eos Trans. AGU 81, 19.

Burr, D.M., McEwen, A.S., Lanagan, P.D., 2000. Recent fluvial activity in and near Marte Vallis, Mars. Lunar Planet. Sci. XXXI. Abstract 1951.

Cabrol, N.A., Grin, E.A., Landheim, R., Kuzmin, R.O., Greeley, R., 1998. Duration of the Ma'adim Vallis/Gusev Crater hydrogeologic system, Mars. Icarus 133, 98–108.

Carr, M.H., 1981. The surface of Mars. Yale Univ. Press, New Haven, CT. 232 p.

Carr, M.H., 1996. Water on Mars. Yale Univ. Press, New York.

Chapman, M.G., Tanaka, K.L., 2002. Related magma–ice interactions: possible origins of chasmata, chaos, and surface materials in Xanthe, Margaritifer, and Meridiani Terrae, Mars. Icarus 155, 324–339.

Christensen, P.R., 1986. The spatial distribution of rocks on Mars. Icarus 68, 217–238.

Christensen, P.R., 16 colleagues, 2000. Detection of crystalline hematite mineralization on Mars by the Thermal Emission Spectrometer: evidence for near-surface water. J. Geophys. Res. 105, 9623–9642.

Christensen, P.R., Morris, R.V., Lane, M.D., Bandfield, J.L., Malin, M.C., 2001. Martian hematite mineral deposits: remnants of water-driven processes on early Mars. J. Geophys. Res. 106, 23873–23885.

Christensen, P.R., 22 colleagues, 2003. Morphology and composition of the surface of Mars: Mars Odyssey THEMIS results. Science 300, 2056–2061.

Christensen, P.R., 11 colleagues, 2004. The Thermal Emission Imaging System (THEMIS) for the Mars 2001 Odyssey Mission. Space Sci. Rev. 110, 85–130.

Crisp, J.A., Adler, M., Matijevic, J.R., Squyres, S.W., Arvidson, R.E., Kass, D.M., 2003. Mars Exploration Rover mission. J. Geophys. Res. 108, 8061.

Crumpler, L.S., Tanaka, K.L., 2003. Geology and MER target site characteristics along the southern rim of Isidis Planitia, Mars. J. Geophys. Res. 108, 8080.

Edgett, K.S., 1997. Nature and source of low-albedo surface material in the sandy aeolian environment of Sinus Meridiani, Mars. Abstracts with Programs, Geological Society of America Annual Meeting 29, A214.

Figueredo, P.H., Greeley, R., 2000. Local variations in aeolian deposits in Melas Chasma, Mars. Lunar Planet. Sci. XXXI. Abstract 1024.

Frey, H., Jarosewich, M., 1982. Subkilometer martian volcanoes: properties and possible terrestrial analogs. J. Geophys. Res. 87, 9867–9879.

Golombek, M.P., 22 colleagues, 2003. Selection of the Mars Exploration Rover landing sites. J. Geophys. Res. 108, 8072.

Greeley, R., Guest, J.E., 1987. Geologic map of the eastern equatorial region of Mars. U.S. Geol. Surv. Misc. Invest. Ser. Map I-1802-B.

Greeley, R., Kuzmin, R.O., Nelson, D.M., Farmer, J.D., 2003a. Eos Chasma, Mars: regional setting for a potential landing site for astrobiology. J. Geophys. Res. 108, 8083.

Greeley, R., Kuzmin, R.O., Rafkin, S.C., Michaels, T.I., Haberle, R., 2003b. Wind-related features in Gusev Crater, Mars. J. Geophys. Res. 108, 8077.

Grin, E.A., Cabrol, N.A., 1997. Limnologic analysis of Gusev Crater paleolake, Mars. Icarus 130, 461–474.

Grizzaffi, P., Schultz, P.H., 1989. Isidis basin: site of ancient volatile-rich debris layer. Icarus 77, 358–381.

Guest, J.E., Greeley, R., 1977. Geology on the Moon. Wykeham, New York.

Head, J.W., Kreslavsky, M.K., Pratt, S., 2002. Northern lowlands of Mars: evidence for widespread volcanic flooding and tectonic deformation in the Hesperian Period. J. Geophys. Res. 107 (E1).

Hynek, B.M., Arvidson, R.E., Phillips, R.J., 2002. Geologic setting and origin of Terra Meridiani hematite deposit on Mars. J. Geophys. Res. 107 (E10), 5088.

Kass, D.M., Schofield, J.T., Michaels, T.I., Rafkin, S.C., Richardson, M.I., Toigo, A.D., 2003. Analysis of atmospheric mesoscale models for entry, descent, and landing. J. Geophys. Res. 108, 8090.

Keszthelyi, L.P., McEwen, A.S., Thordarson, T., 2000. Terrestrial analogs and thermal models for martian flood lavas. J. Geophys. Res. 105, 15027–15049.

Kirk, R.L., Howington-Kraus, A., Redding, B., Galuszka, D., Hare, T.M.A., Archinal, B., Soderblom, L.A., Barret, J.M., 2003. High-resolution topomapping of candidate MER landing sites with Mars Orbiter Camera narrow-angle images. J. Geophys. Res. 108, 8088.

Koeppen, W.C., Seelos IV, F.P., Arvidson, R.E., Christensen, P.R., 2003. Terrain distributions in Meridiani Planum and probability of sampling by the Mars Exploration Rover. Lunar Planet. Sci. XXXIV. Abstract 1853 [CD-ROM].

Komatsu, G., Geissler, P.E., Strom, R.G., Singer, R.B., 1993. Stratigraphy and erosional landforms of layered deposits in Valles Marineris. J. Geophys. Res. 98, 11105–11121.

Kuzmin R.O., Greeley R., Landheim R., Cabrol N.A., Farmer J.D., 2000. Geologic map of the MTM-15182 and MTM-15187 quadrangles, Gusev Crater–Ma'adim Vallis Region, Mars. Geologic Investigative Series, U.S. Geological Survey, Reston, VA.

Kuzmin R.O., Greeley R., Nelson D., Farmer J.D., Klein C., 2001. Eos Chasma and NE Valles Marineris. In: 2nd MER 2003 Landing Site Workshop.

Lanagan P.D., McEwen A.S., 2003. Cerberus Plains volcanism: constraints on temporal emplacement of the youngest flood lavas on Mars. In: Sixth International Conference on Mars. Abstract 3215 [CD-ROM].

Lucchitta, B.K., 1982. Ice sculpture in the martian outflow channels. J. Geophys. Res. 87, 9951–9973.

Lucchitta, B.K., 1987. Valles Marineris, Mars—wet debris flows and ground ice. Icarus 72, 411–429.

Lucchitta, B.K., Isbell, N.K., Howington-Kraus, A., 1994. Topography of Valles Marineris: implications for erosional and structural history. J. Geophys. Res. 99, 3783–3798.

Malin, M.C., Edgett, K.S., 2000. Sedimentary rocks of early Mars. Science 290, 1927–1937.

Mellon, M.T., Jakosky, B.M., Kieffer, H.H., Christensen, P.R., 2000. High-resolution thermal inertia mapping from the Mars Global Surveyor Thermal Emission Spectrometer. Icarus 148, 437–455.

Milam, K.A., Stockstill, K.R., Moersch, J.E., McSween Jr., H.Y., Tornabene, L.L., Ghosh, A., Wyatt, M.B., Christensen, P.R., 2003. THEMIS characterization of the MER Gusev Crater landing site. J. Geophys. Res. 108, 8078.

Nedell, S.S., Squyres, S.W., Anderson, D.W., 1987. Origin and evolution of the layered deposits in the Valles Marineris, Mars. Icarus 70, 409–441.

Newsom, H.E., Barber, C.A., Hare, T.M., Schelble, R.T., Sutherland, V.A., Feldman, W.C., 2003. Paleolakes and impact basins in southern Arabia Terra, including Meridiani Planum: implications for the formation of hematite deposits on Mars. J. Geophys. Res. 108, 8075.

Nowicki S., Christensen P.R., 2002. Rock abundance derived from TES data. In: 3rd 2003 Mars Exploration Rovers Landing Site Selection Workshop.

Palluconi, F.D., Kieffer, H.H., 1981. Thermal inertia mapping of Mars from 60° S to 60° N. Icarus 45, 415–426.

Parker, T.J., Saunders, R.S., Schneeberger, D.M., 1989. Transitional morphology in west Deuteronilus Mensae, Mars: implications for modification of the lowland/upland boundary. Icarus 82, 111–145.

Parker, T.J., Gorsline, D.S., Saunders, R.S., Pieri, D.C., Schneeberger, D.M., 1993. Coastal geomorphology of the martian northern plains. J. Geophys. Res. 98, 11061–11078.

Pelkey, S.M., Jakosky, B.M., 2002. Surficial geologic surveys of Gale Crater and Melas Chasma, Mars: integration of remotes-sensing data. Icarus 160, 228–257.

Pelkey, S.M., Jakosky, B.M., Christensen, P.R., 2003. Surficial properties in Melas Chasma, Mars, from Mars Odyssey THEMIS data. Icarus 165, 68–89.

Peulvast, J.P., Masson, P.L., 1993. Erosion and tectonics in Central Valles Marineris (Mars). A new morpho-structural model. Earth Moon Planets 61, 191–217.

Plescia, J.B., 1980. Cinder cones of Isidis and Elysium. Reports of Planetary Geology Program NASA TM-82358, 263–265.

Plescia, J.B., 2003. Cerberus Fossae, Elysium, Mars: a source for lava and water. Icarus 164, 73–95.

Presley, M.A., Arvidson, R.E., 1988. Nature and origin of materials exposed in the Oxia Palus–Western Arabia–Sinus Meridiani region, Mars. Icarus 75, 499–517.

Rafkin, S.C., Michaels, T.I., 2003. Meteorological predictions for 2003 Mars Exploration Rover high-priority landing sites. J. Geophys. Res. 108, 8091.

Ruff, S.W., Christensen, P.R., 2002. Bright and dark regions on Mars: particle size and mineralogical characteristics based on Thermal Emission Spectrometer data. J. Geophys. Res. 107 (E12), 5127.

Sakimoto, S.E.H., Riedel, S.J., Burr, D.M., 2001. Geologically recent martian volcanism and flooding in Elysium Planitia and Cerberus Rupes: plains-style eruptions and related water release? Geological Society of America Abstracts with Programs 33, A431.

Scott, D.H., Tanaka, K.L., 1986. Atlas of Mars: 1:15,000,000 Geologic Series, Western Region. U.S. Geol. Surv. Misc. Invest. Map 1802-A.

Scott, D.H., Tanaka, K.L., Greeley, R., Guest, J.E., 1987. Geologic maps of the western and eastern equatorial and polar regions of Mars. U.S. Geol. Surv. Misc. Invest. Ser. Map I-1802-A, B, C.

Sharp, R.P., 1973. Mars: trough terrain. J. Geophys. Res. 78, 4063–4072.

Skilling, I.P., Chapman, M.G., Lucchitta, B.K., 2002. Young, blocky flows in east Ius/west Melas and west Candor Chasmata, Mars: debris avalanche deposits derived from interior layered deposit (ILD) mounds? Lunar Planet. Sci. XXXIII. Abstract 1361.

Squyres, S.W., 12 colleagues, 2003. Athena Mars rover science investigation. J. Geophys. Res. 108, 8082.

Tanaka, K.L., 1997. Sedimentary history and mass flow structures of Chryse and Acidalia Planitiae, Mars. J. Geophys. Res. 102, 4131–4150.

Tanaka, K.L., Skinner Jr., J.A., Hare, T.M., Joyal, T., Wenker, A., 2003. Resurfacing history of the northern plains of Mars based on geologic mapping of Mars Global Surveyor data. J. Geophys. Res. 108, 8043.

Weitz, C.M., Parker, T.J., Bulmer, M.H., Anderson, F.S., Grant, J.A., 2003. Geology of the Melas Chasma landing site for the Mars Exploration Rover mission. J. Geophys. Res. 108, 8082.

Witbeck, N.E., Tanaka, K.L., Scott, D.H., 1991. Geologic map of the Valles Marineris region, Mars. U.S. Geol. Surv. Misc. Invest. Ser. Map I-2010.